Seismic evidence for Neogene and active shortening offshore of Lebanon (Shalimar cruise)

H. Carton,[1,2] S. C. Singh,[1] P. Tapponnier,[3] A. Elias,[1,4,5] A. Briais,[6] A. Sursock,[4] R. Jomaa,[4] G. C. P. King,[3] M. Daëron,[7] E. Jacques,[3] and L. Barrier[3]

Received 20 September 2007; revised 10 November 2008; accepted 20 April 2009; published 24 July 2009.

[1] Lebanon, located on a 160-km-long transpressional bend of the left-lateral Levant (Dead Sea) fault system (LFS), has been the site of infrequent but large earthquakes, including one submarine, tsunamigenic event. The main objective of the Shalimar marine survey was to characterize and map active deformation offshore of Lebanon using a range of geophysical techniques, particularly seismic reflection profiling. The cruise results clearly establish the presence of young submarine thrust faults and folds and clarify the structure of this part of the Levant margin. A submarine fold belt, bounded by thrusts and lateral ramps and extending up to 30 km from the shoreline, is interpreted as the foreland thrust system of the actively growing Mount Lebanon range. There is no large fault extending into the Levant basin toward Cyprus, which indicates that thrusting only absorbs local transpression resulting from the Lebanese restraining bend. Both the Miocene and Plio-Quaternary sedimentary sequences are affected by shortening, with landward dipping blind thrusts and associated growth strata. The presence of the Messinian evaporites creates complex deformation patterns, including normal faults due both to folding accommodation and to gravity spreading, all well imaged in the seismic reflection profiles. Because the evaporite layer acts as a décollement level, shortening extends farther out seaward through a series of thrust imbricates or duplexes. The strongest shortening, observed between Beirut and Batroun, decreases toward the south between Saida and Tyre. North of Tripoli, the passive margin is not affected by Neogene deformation and is well preserved. We propose that since the Miocene, the northward propagating LFS interacted with margin structures inherited from the Mesozoic rifting phase and was deviated along the more rigid oceanic crust flooring the Levant basin, a process which led to the formation of the Lebanese restraining bend of the LFS and consequently to the offshore shortening we document here. Such coastal transpression has resulted in local (~100 km) inversion of the passive margin, which might eventually evolve into a new subduction zone.

Citation: Carton, H., et al. (2009), Seismic evidence for Neogene and active shortening offshore of Lebanon (Shalimar cruise), *J. Geophys. Res.*, *114*, B07407, doi:10.1029/2007JB005391.

1. Introduction

1.1. Levant Fault System

[2] The Levant fault system (LFS) is the ~1000-km-long left-lateral transform that accommodates the northward motion of the Arabian plate relative to the Sinai-Levantine subplate. It extends between the Gulf of Aqaba, at the northern termination of the Red Sea, and the Taurus mountains in southern Turkey (Figure 1). In its southern part, for over 450 km, as well as in its northernmost stretch, the LFS has a north–south orientation and is segmented by extensional (left-stepping) step overs, which are occupied by pull-apart basins (Gulf of Aqaba, Dead Sea, and Ghab basin). In between, the Lebanese restraining bend forms the most conspicuous irregularity along the LFS. Here the orientation of the fault rotates 25° clockwise over a distance of ~150 km.

[3] Sinistral shear along the western side of Arabia is a consequence of the opening of the Red Sea, since 25–30 Ma ago, between the Arabian and Nubian plates [e.g., *Courtillot et al.*, 1987; *Manighetti et al.*, 1998, and references therein]. Strike-slip motion along the LFS is believed to have started in the Miocene, 15–18 Ma ago. The total

[1]Equipe de Géosciences Marines, Institut de Physique du Globe de Paris, Paris, France.
[2]Now at Lamont-Doherty Earth Observatory, Earth Institute at Columbia University, Palisades, New York, USA.
[3]Equipe de Tectonique, Institut de Physique du Globe de Paris, Paris, France.
[4]National Center for Geophysical Research, Beirut, Lebanon.
[5]Now at Geology Department, American University of Beirut, Beirut, Lebanon.
[6]Laboratoire de Dynamique Terrestre et Planétaire, Observatoire Midi-Pyrénées, Toulouse, France.
[7]Laboratoire des Sciences du Climat et de l'Environnement, Gif-sur-Yvette, France.

0148-0227/09/2007JB005391$09.00

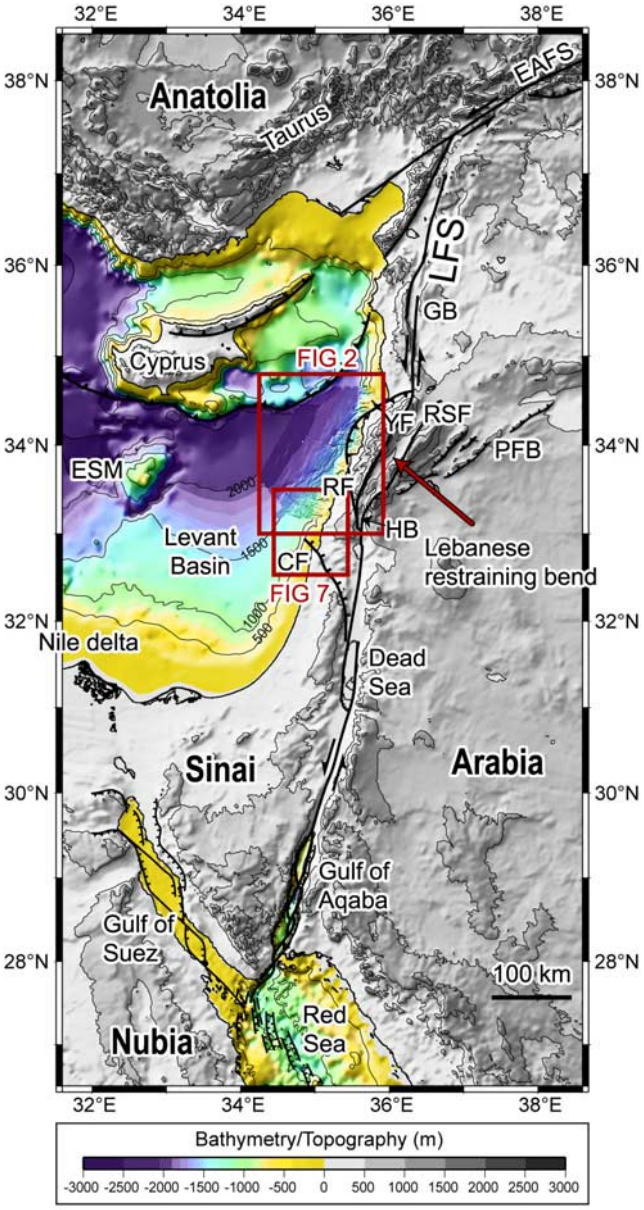

Figure 1. Regional map of Levant area and Levant fault system (LFS), modified after *Daëron et al.* [2004]. Topography is from GEBCO 1-min grid with Shalimar survey bathymetry superimposed; contours are every 500 m. Boxes show locations of Figures 2 and 7. EAFS, East Anatolian fault system; ESM, Eratosthenes Seamount; YF, Yammouneh fault; RSF, Rachaya-Serghaya fault; RF, Roum fault; PFB, Palmyrides fold belt; GB, Ghab basin; CF, Carmel fault; HB, Hula basin.

cumulative offset is generally accepted to be ~105 km south of 32°N [e.g., *Freund et al.*, 1968, 1970; *Garfunkel*, 1981; A. M. Quennell, Tectonics of the Dead Sea rift, paper presented at 20th International Geological Congress, Asociacion de Servicios Geologicos Africanos, Mexico City, 1959]. The present-day slip rate along the LFS has been estimated to be 4–10 mm/a on the basis of plate tectonic models [e.g., *Joffe and Garfunkel*, 1987; *DeMets et al.*, 1994; *Chu and Gordon*, 1998] or early GPS observations [*McClusky et al.*, 2003]. However, most plate tectonic and GPS models describe the Arabia/Nubia plate motion, neglecting the small divergent motion across the Gulf of Suez, the southwestern boundary of the Sinai subplate. A new GPS study focusing on the boundaries of the Sinai block provided revised geodetic slip rate estimates of 4.1–4.7 mm/a on the southern part of the LFS and 3–3.8 mm/a, with a component of shortening, along the Lebanese restraining bend [*Mahmoud et al.*, 2005]. Recently, *Daëron et al.* [2004] obtained a slip rate of 3.8–6.4 mm/a in the last ~25 ka from cosmogenic exposure dating of offset alluvial fans along the Yammouneh fault in Lebanon.

[4] Available instrumental records, which show a rather low level of recent seismicity on the LFS, are not representative of the long-term seismicity affecting this area [*Guidoboni et al.*, 2004]. Large (Ms > 7.0) but relatively infrequent earthquakes are known to have struck Israel, Palestine, Lebanon and Syria in earlier centuries [*Ambraseys and Barazangi*, 1989; *Khair*, 2001]. In Lebanon, the strongest earthquakes of the past two millenia occurred in 551 AD [*Elias et al.*, 2007], 1202 AD [*Daëron et al.*, 2005, 2007], and October and November 1759 AD [*Ambraseys and Barazangi*, 1989; *Gomez et al.*, 2003; *Daëron et al.*, 2005].

1.2. Lebanese Restraining Bend

[5] Transpression within the Lebanese bend has been responsible for the formation of the highest mountains of the Near East, including Mount Lebanon (3083 m), Mount Hermon (2814 m), and the Anti-Lebanon (2629 m) [e.g., *Dubertret*, 1955]. Comparably high relief is absent south or north of the bend, where the direction of the LFS is roughly N–S. East of the Lebanese restraining bend, the Palmyrides fold belt presently accommodates internal deformation within the Arabian plate [*Chaimov et al.*, 1990]. The growth of the Lebanese ranges has been inferred to have started in the Cretaceous [e.g., *Dubertret*, 1955; *Walley*, 1998], and has been related to the Eocene Syrian Arc tectonic phase, which generated shortening in other areas of the Levant [e.g., *Ginzburg et al.*, 1975; *Walley*, 1998] (seismic data examples of *Frey Martinez et al.* [2005] and *Bertoni and Cartwright* [2006]). Recent fieldwork, however, has shown crustal shortening and mountain building in Lebanon to be much more recent, initiating only ~10–15 Ma ago [*Elias*, 2006]. Moreover, there is strong evidence for recent and ongoing shoreline uplift along the coast, most prominently between Beirut and Tripoli [*Sanlaville*, 1977; *Morhange et al.*, 2006; *Elias et al.*, 2007]. There, uplifted bioconstructions appear to have recorded coseismic uplift during the 551 AD earthquake, whose source was located offshore [*Elias et al.*, 2007].

[6] The LFS splays into several branches within the Lebanese restraining bend area (Figure 1). Strike-slip segments south and north of the bend are connected through the SW–NE trending, left-lateral Yammouneh fault (3.8–6.4 mm/a [*Daëron et al.*, 2004]). The subparallel Rachaya-Serghaya fault (1–1.5 mm/a slip rate from paleoseismologic studies [*Gomez et al.*, 2003]) and the SSE–NNW trending Roum fault (1 mm/a slip rate from paleoseismologic studies [*Nemer and Meghraoui*, 2006]) are two secondary left-lateral branches that split off the LFS near the Hula basin at the southern extremity of the bend (Figure 1). Since motion is purely strike slip along the Yammouneh and

Rachaya-Serghaya faults [e.g., *Daëron et al.*, 2004], NW–SE shortening within the bend ought to be accommodated on thrust faults, associated with the growth of the Lebanese ranges. On the basis of the identification of active thrust faults in the Tripoli region, *Tapponnier et al.* [2001] and *Elias* [2006] proposed the existence of a large thrust fault system (MLT, Mount Lebanon Thrust) underlying the Lebanese flexure, which would reach the surface in the offshore area between the cities of Saida and Tripoli. The need for structures taking up the convergent component of motion within the bend has since then been acknowledged [e.g., *Nemer and Meghraoui*, 2006; *Gomez et al.*, 2007], but none had been adequately mapped prior to the Shalimar survey.

1.3. Levant Basin and Margin

[7] Facing the Lebanese mountain is the Levant basin (2000-m water depth), the easternmost basin of the Mediterranean Sea. It is bounded to the south and to the east by the Levant margin, along the coasts of Libya, Egypt, Israel, Lebanon, and Syria, and to the north by the Cyprus arc, the easternmost segment of the East Mediterranean subduction zone [e.g., *McKenzie*, 1972] (Figure 1). Between the Israeli and Libyan coasts the basin is partly covered by the thick deep-sea fan of the Nile delta. Despite some debate about the nature of the crust underlying the Levant basin, it is generally accepted that this basin is a relict of the Mesozoic Neotethys ocean [*Ryan et al.*, 1970; *Dercourt et al.*, 1986; *Ben-Avraham*, 1989; *Ricou*, 1995; *Garfunkel*, 1998], which has been consumed by subduction in the north. Modeling of refraction profiles shot offshore of Israel [*Makris et al.*, 1983; *Ben-Avraham et al.*, 2002] suggests the presence of an 8-km-thick oceanic crust (6.7–6.8 km/s) beneath a 12- to 14-km-thick sedimentary sequence. An alternative model is one with a two-layered crystalline basement of attenuated continental nature, with velocities of 6.0–6.4 and 6.5–6.9 km/s, respectively [*Netzeband et al.*, 2006a]. The thick sedimentary sequence includes a high-velocity evaporite layer (4.2 km/s from refraction modeling), up to 2 km thick, deposited during the Messinian dessication episode [*Ben-Avraham et al.*, 2002; *Netzeband et al.*, 2006a]. Levant continental margin appears to have been shaped by several faulting episodes [*Garfunkel*, 1998, 2004]. Evidence for Triassic rifting and regional thinning of the crust exists in southern Israel and in the Palmyrides, where grabens formed in response to NW–SE extension. A second episode of extension at the end of the Jurassic and at the beginning of the Cretaceous (140–110 Ma) likely led to seafloor spreading in the Levant basin [*Dercourt et al.*, 1986; *Ricou*, 1995]. The petrology of 150–100 Ma old basalts in Lebanon, Syria and Israel (Bhannes-Tayasir basalts), typical of rifting [*Laws and Wilson*, 1997], confirms the importance of this Late Jurassic rifting phase. So does the existence of ENE–WSW trending normal faults affecting strata older than Upper Cretaceous in the central part of Mount Lebanon [*Dubertret*, 1955]. Such large-scale block faulting established the final structure and geometry of the Levant passive margin under a NNW–SSE extensional regime.

1.4. Active Deformation Offshore of Lebanon

[8] The recent tectonic evolution of offshore Lebanon has been a subject of wide-ranging speculations. Several hypotheses were put forward, postulating recent or active motion on one or several submarine faults. *Girdler* [1990] first suggested that the main transform boundary continued from south of Beirut toward Cyprus, following a small circle of the Arabia/Africa rotation. *Butler et al.* [1997] further proposed that the Roum fault was in fact the most recent location of the plate boundary, the Yammouneh fault being no longer active. But it has now been unambiguously demonstrated that active strike-slip motion is transferred to the northern part of the LFS in Syria through the Yammouneh fault [*Daëron et al.*, 2004, 2005, 2007] and hence that it is unlikely that the Arabia/Sinai plate boundary lies within the Levant basin. On the other hand, it has long been noticed [*Ben-Avraham and Hall*, 1977; *Ben-Avraham*, 1978; *Nur and Ben-Avraham*, 1978] that the southern Levant margin offshore of Israel shows smooth bathymetry with a relatively broad continental shelf (~20–25 km), while the margin becomes narrower and steeper to the north, along the Lebanese coast. The same authors suggested that a strike-slip deformation zone might run subparallel to the coast of Lebanon and that the Carmel fault might be a major boundary, extending at sea, between the southern and northern parts of the basin. Even more elaborate interpretations were recently proposed by *Ben-Avraham et al.* [2006] and *Schattner et al.* [2006], based on the analysis of previously unpublished single-channel and newly acquired seismic data offshore of Israel. A marine geophysical survey was therefore required to test these various hypotheses and shed light onto the neotectonics of offshore Lebanon.

2. Data Acquisition and Processing

[9] In the fall of 2003, the Shalimar marine survey (complemented by Shaliban) was conducted as part of a French-Lebanese collaborative program to study recent deformation along the Lebanese margin of the Levant basin (Figure 2). The main objectives were to study the deformation of recent sedimentary layers, map potentially active faults on the seafloor, and identify possible seismic ruptures. A variety of geophysical techniques were used to achieve these goals, including high-resolution multibeam bathymetry and short-streamer seismic profiling. High-speed six-channel seismics, as part of a reconnaissance work, was followed by high-resolution 24-channel seismics (~1 s penetration) focusing on previously identified targets.

[10] Bathymetric mapping was carried out using a Simrad EM-300 multibeam echo sounder providing high-resolution bathymetric and backscatter data, at a vessel speed of 7.5 to 10 knots. In order to achieve a uniform coverage, the sail lines were parallel to the coast, spaced up to 4–5 km apart. Seismic reflection data were simultaneously acquired, followed by a set of E–W lines shot with the same equipment, extending up to 70 km from the coast in the central offshore area. This provided a grid of profiles at 4- to 5-km spacing, numbered from 1 to 90, which amounts to about 3000 km of high-speed (HS) data. The seismic source for the HS acquisition consisted of two GI guns with capacities of 45/45 a 105/105 cubic inches, towed at 6-m depth. The conventional approach of enhancing the primary peak was used, providing a broadband (8–75 Hz) source response. The data were recorded on a six-channel streamer towed at 5-m depth with 50-m hydrophone group spacing. The

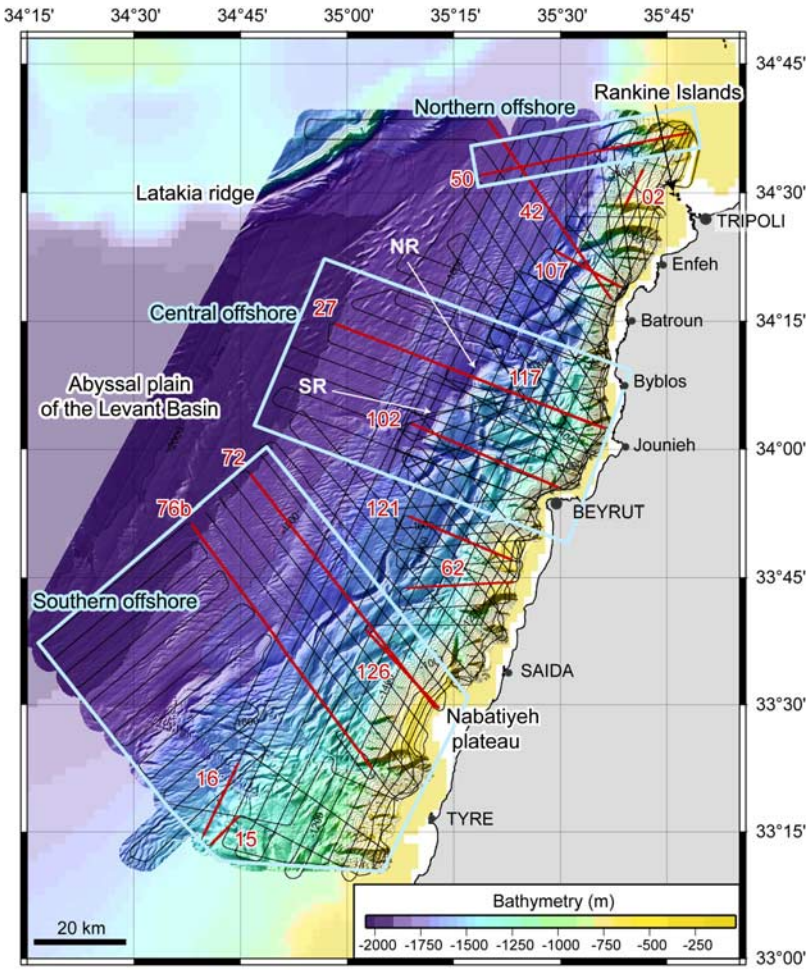

Figure 2. New bathymetric map of offshore Lebanon. Data were recorded using an EM-300 Simrad multibeam system, over an area of 11,000 km^2. Grid has 100-m pixel size; contours are every 100 m. Track lines along which seismic reflection data were acquired are shown in black. Profiles or portions of profiles discussed in text are marked by thick red lines (HS-50, 02, 42, 27, 62, 72, 76b, 15, 16: high-speed, six-channel seismic system; HR-107, 117, 102, 121, 126: high-resolution, 24-channel seismic system). Blue boxes indicate three main domains of offshore Lebanon, where contrasting deformation patterns are observed. NW corner of study area encroaches upon Latakia ridge, southeast of Cyprus subduction zone. SR, southern ridge; NR, northern ridge.

acquisition geometry for HS seismics yielded a common midpoint (CMP) spacing of 25 m with three traces per CMP gather. On the basis of the new bathymetric map and preliminary onboard processing of the HS seismic data, a further 700 km of high-resolution data were acquired, with line numbers ranging from 101 to 126. The high-resolution (HR) system was operated with a vessel speed of 4.5 to 5 knots. The source consisted of six miniGI guns with capacities of 13/13 and 24/24 cubic inches, towed at 1.5-m depth, and energy was maximum between 12 and 160 Hz. The data were recorded on a 300-m-long, 24-channel streamer with 12.5-m hydrophone group spacing and towed at 3-m depth. The acquisition geometry for HR seismics yielded a CMP spacing of 6.25 m with either 6 or 10 traces per CMP gather. The HR profiles provided a fine-scale sampling of central offshore Lebanon, whereas high-speed profiles were shot as a dense grid within the whole survey area.

[11] Processing was carried out using the Focus software. The main steps for processing of HS seismic data were geometry definition, frequency filtering (corner frequencies 14-18-75-80 Hz), stacking, and constant-velocity (Stolt) migration. Migration was very useful to collapse the numerous diffraction hyperbolae of the stack section. A 1700 m/s velocity value provided an acceptable compromise to migrate the whole section. A similar processing sequence was applied to HR data (filtering with corner frequencies 55-60-230-250 Hz) but 2-D Kirchhoff migration was applied in order to get the best focused images. For each HR line, a 2-D velocity model was built using several interfaces picked with the line-based interpretation package SeisX: the seafloor, and the M horizon in deep water, which continues landward as an erosional surface on the continental slope and platform. The M horizon, which is a well-known stratigraphic marker in the eastern Mediterranean [*Ryan et al.*, 1970], marks the boundary between Plio-Quaternary sediments and higher-velocity Messinian evaporites. It migrated best for velocities ranging from ~1550 to ~1700 m/s, depending upon the location. The overlying

turbiditic layer is dissected by numerous small-throw faults, originating at the top of the evaporites, and velocities were locally adjusted in order to obtain the sharpest images of these faults. The subset of profiles discussed in this paper are shown with a vertical exaggeration of four at the seabed. The uninterpreted HR profiles are displayed with an AGC gain (window length 200 ms) to enhance deep features.

[12] The sedimentary pile in the survey area comprises a layer of evaporites deposited during the Messinian salinity crisis. This evaporitic layer appears to have been deformed through shortening and salt tectonics processes, resulting in the formation of rafts, rollovers, folds, diapers, and elongated salt walls. Seismic reflection imaging in thrust and salt environments is known to be particularly challenging, because of lateral velocity variations produced by the juxtaposition of high-velocity salt bodies and lower velocity rocks. The geometric assumptions (horizontally layered media) upon which standard time processing rests break down in such environments, thus producing distorted images, the interpretation of which can be difficult. In order to image reservoirs located beneath complex geological structures such as salt diapirs and folds, the oil industry has adopted depth processing techniques, especially prestack depth migration [e.g., *Fagin*, 1998]. It was, however, not possible to apply such advanced processing methods to the short-streamer data from the Shalimar survey. The situation is also rendered more complex by the fact that 3-D effects likely perturb the 2-D seismic sections. Therefore, special care was taken in interpreting the Shalimar poststack time-migrated images, bearing in mind that the interpretation must be geologically meaningful and that overinterpretation should be avoided.

3. Seafloor Morphology

[13] The water depth in the survey area globally increases westward, from 50 to 100 m nearshore to 2000 m in the abyssal plain of the Levant basin (Figure 2). The continental shelf is relatively wide in the north, offshore of the Akkar plain (about 20 km), and in the south, offshore of Saida and Tyre (Nabatiyeh plateau). Between Beirut and Batroun however, the shelf is extremely narrow and the margin exhibits its steepest slope, with the water depth abruptly increasing from 100 to 1500 m in less than 5 km. As documented below, the base of this sharp topographic step is likely the site where steeply east dipping thrust ramps underlying the Lebanese ranges rise closest to or even emerge on the seafloor. Along the entire margin the continental slope is incised by canyons, most of them connected to rivers flowing from the mountains. Between 1500- and 1800-m water depth, the seafloor is perturbed by elongated features that are characteristic of two main areas, a triangle-shaped area extending southwest of Beirut, and offshore of Beirut-Batroun, up to 30 km from the coastline. Among these structures, those oriented roughly parallel to the coast are either diverted submarine channels, elongated troughs, or submarine ridges. Two such ridges that are discussed in greater detail using seismic reflection profiles are located offshore of Enfeh and Batroun, about 30 km from the shore (southern ridge (SR) and northern ridge (NR) in Figure 2). In the northwestern part of the survey area, anticlinal ridges corresponding to the deformation front of the Cyprus subduction zone are imaged, with the Latakia ridge culminating about 700 m above the basin floor. The detailed description and interpretation of the seafloor morphology are presented and discussed by *Elias* [2006] and A. Elias et al. (manuscript in preparation, 2009).

4. Stratigraphy of Offshore Lebanon From Seismic Profiles and Previous Data

[14] The Shalimar seismic profiles sample the first few kilometers of sediments, down to the first seafloor multiple. The stratigraphy is best defined on the northernmost profile (profile HS-50, Figure 3), north of Tripoli, offshore Akkar plain. This profile was specifically designed to avoid the predicted offshore extension of the Lebanese restraining bend deformation zone (e.g., tectonic map of *Daëron et al.* [2004], Figure 1)), in an attempt to image the undeformed Levantine margin. Correlations of major reflectors can be easily established between the western end of this profile, at 1800-m water depth, and the N–S depth sections from *Vidal et al.* [2000] and the time sections of *Hall et al.* [2005], both of which extend south of the Cyprus subduction zone into the Levant basin west of Lebanon. In the south, our interpretation of the offshore stratigraphy is consistent with published interpretations of data acquired offshore of Israel, such as single-channel profiles [*Ben-Avraham*, 1978], extensive oil industry data [*Bertoni and Cartwright*, 2006], and shallow seismic profiles acquired by the German *Meteor* vessel in 2002 [*Gradmann et al.*, 2005; *Netzeband et al.*, 2006b]. There is, however, no available offshore well data within or close to the Shalimar survey area that could provide information about sediment nature and direct measurements of thicknesses and seismic velocities. The closest ODP boreholes are located between the Eratosthenes Seamount and Cyprus [*Robertson et al.*, 1996], in an area of incipient continental collision, and may not be representative of the rest of the Levant basin. The stratigraphy observed in the Shalimar seismic profiles is described below [see also *Elias*, 2006; A. Elias et al., manuscript in preparation, 2009].

[15] The topmost deep-water deposits, which are well imaged along the Lebanese margin and reach thicknesses of 1.4 s in places, form a distinctive, finely bedded sequence. These deposits are probably mostly turbidites, especially in the distal part, with perhaps also some hemipelagites. Sand waves are imaged as very shallow west dipping discontinuities, especially within the thickest sedimentary piles. The strong reflector that marks the base of this uppermost unit is readily interpreted as the M horizon, which is ubiquitous in the Mediterranean [*Ryan et al.*, 1970]. This horizon corresponds to the transgressional unconformity at the top of the Messinian evaporites and base of the Plio-Quaternary deposits that marked the return of the sea. It has a well-constrained age of 5.3 Ma. Where affected neither by folding nor faulting, as on profile 50 (Figure 3), the M horizon is horizontal, at about 2.9 s below the sea level (bsl). Although the HS seismic profiles show mostly one main reflector, HR profiles indicate the presence of a second reflector above, which probably reflects the presence of a transitional layer above the Messinian proper. The main evaporite layer (halite + gypsum) is essentially transparent but some internal reflectors are visible. Offshore of Israel,

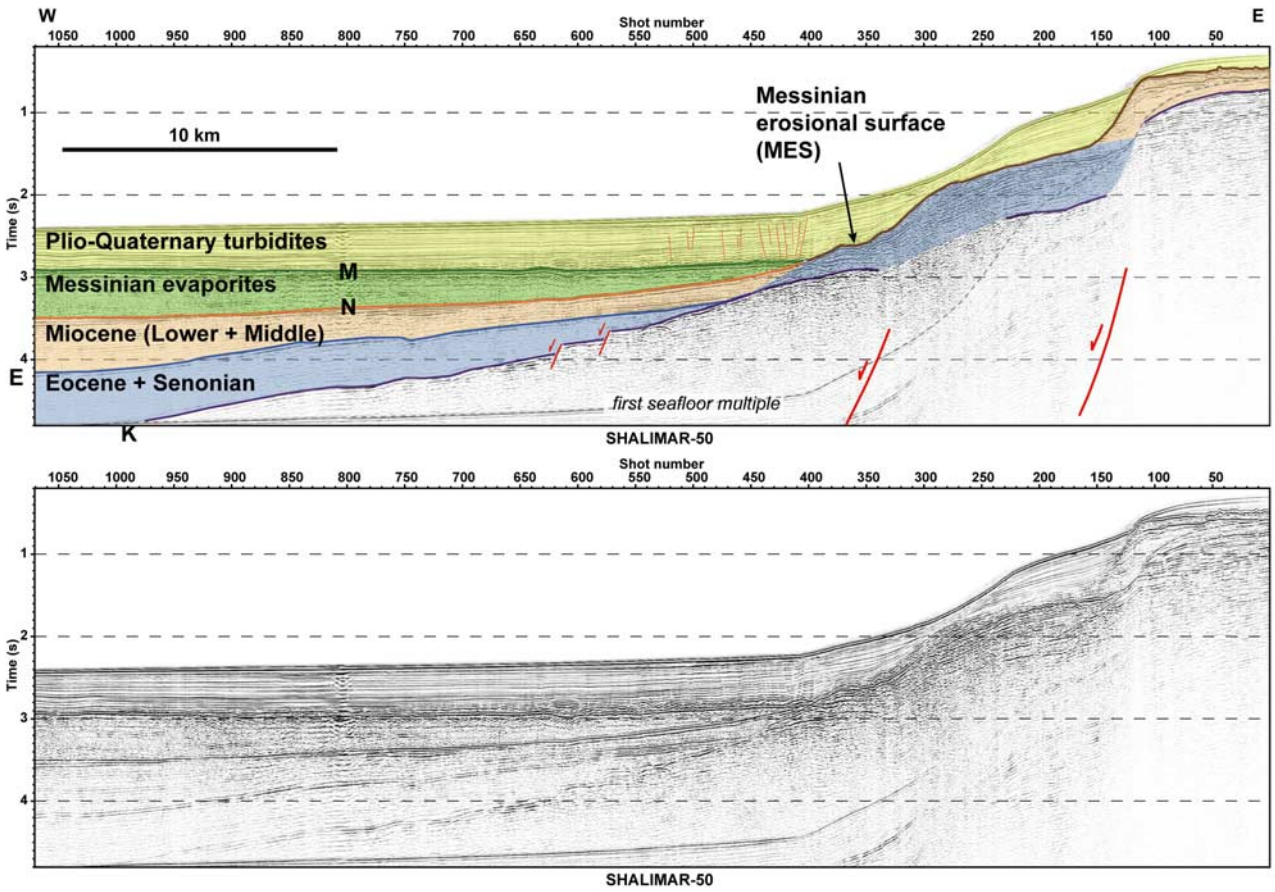

Figure 3. Profile HS-50 in northern offshore area.

the Messinian layer in deep water has been shown to consist of a stack of five transparent layers bounded by internal reflectors, which can be interpreted either to represent changes of evaporite facies or to mark the presence of intercalated clastic sediments [*Gradmann et al.*, 2005; *Netzeband et al.*, 2006b]. The presence of intercalated sediments within the evaporite layer would result in a decrease of the seismic interval velocity. The next strongest reflector underneath M corresponds to the base of the Messinian evaporites, also called N horizon south of Cyprus [e.g., *Vidal et al.*, 2000]. On the reference profile (Figure 3), the evaporite layer pinches out at 2.9 s bsl where reflectors M and N merge landward into an erosional surface. This surface, which is particularly well imaged on the HR profiles, generally displays a rough topography, sometimes truncating older deposits at sharp angles, and is unconformably overlain by Plio-Quaternary sediments. We interpret this reflector as the Messinian erosional surface (MES), the rocks underneath it being terranes emerged during the Messinian dessication event. Several distinctive reflectors below the evaporites are also well imaged down to 4.5 s bsl in the northwestern part of the survey area where they are not obscured by multiples. As seen on the reference profile (Figure 3), these reflectors define a well-bedded, seaward thickening sedimentary sequence. Two such reflectors that stand out particularly clearly likely represent the base of the Miocene and the base of the Senonian, respectively, an interpretation fully compatible with onshore well data (Terbol-1 well [*Beydoun*, 1977]) and with observations in the Tripoli region [*Dubertret*, 1955; *Elias*, 2006; A. Elias et al., manuscript in preparation, 2009], where these two stratigraphic limits correspond to the most important facies changes in the regional late Mesozoic/Tertiary sedimentary section.

5. Tectonic Deformation From Seismic Profiles

[16] Three areas (northern, southern, and central offshore areas), in which deformation evolves from negligible or small, to moderate, and finally intense, as well as two transition zones between the three main domains (Figure 2), are successively described below.

5.1. Northern Offshore Area (North of Tripoli)

[17] Profile HS-50 north of Tripoli (Figure 3) clearly shows the flat-lying M reflector and N horizon that merge at the base of the continental slope. The Plio-Quaternary sediments above are affected by slight extensional faulting around the evaporite wedge pinch-out. Overall, there is very little deformation of the entire Neogene-Quaternary sedimentary sequence. The Messinian, the lower-middle Miocene, and the Eocene-Senonian layers show clear thickening toward the abyssal plain of the Levant basin. Underneath the margin slope, we infer that two large normal faults are responsible for the steepening of strata and west facing flexures visible in the Senonian sequence around SP 150 and 350. These faults likely shaped the passive margin in

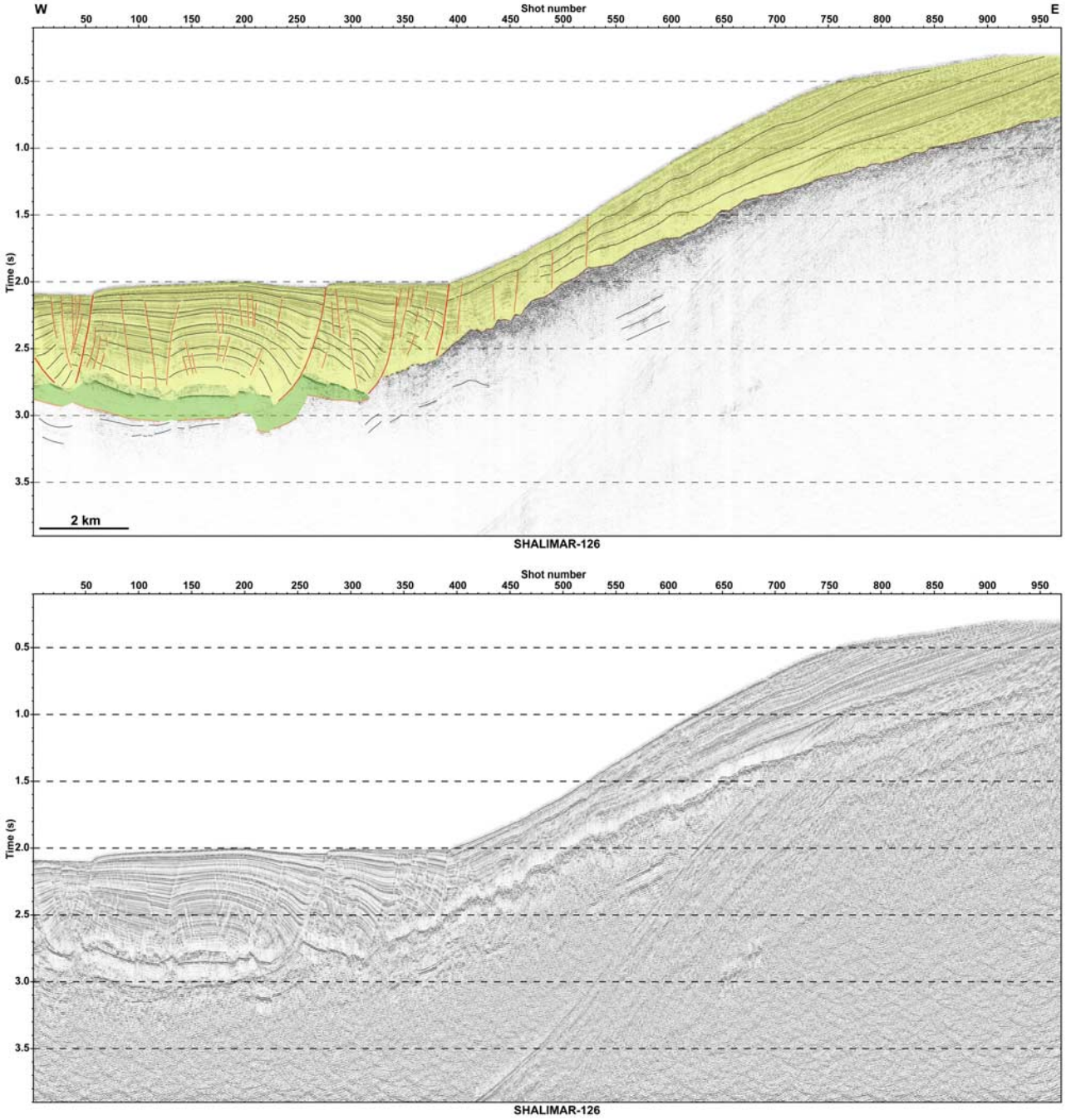

Figure 4. Profile HR-126 in southern offshore area.

the Late Jurassic to Neocomian. Smaller normal offsets are also clear at the top of the mid-Cretaceous (K) farther west.

5.2. Southern Offshore Area (South of Saida)

[18] In the offshore area south of Saida, profile HR-126 (Figure 4) cuts across the edge of the Nabatiyeh plateau. On the plateau area, the erosional surface is overlain by prograding clinoforms of regularly bedded turbidites. Near the base of the slope, the beds are affected by small normal faults. In deeper water, both the evaporite layer and the Plio-Quaternary pile show extensive normal faulting, with many small faults within the turbidites and a few larger ones that cut the evaporitic layer, displacing the M reflector and extending up to the surface. While most of the faults visible only above the evaporite layer have very small throws, a few of those that cut M to reach the surface have much larger offsets that decrease markedly upward. At SP 280 and SP 50, two such faults have created 20- to 30-m-high, west facing, cumulative escarpments on the seafloor. Another large fault is observed at the base of the slope. Such geometry is readily interpreted as the expression of salt tectonics [*Vendeville and Cobbold*, 1987; *Mauduit and Brun*, 1998; *Fort et al.*, 2004], as observed along several passive margins, particularly the west African margin, and the Levant margin offshore of Israel just south of our survey area [*Garfunkel*, 1984, 1998; *Garfunkel and Almagor*, 1987;

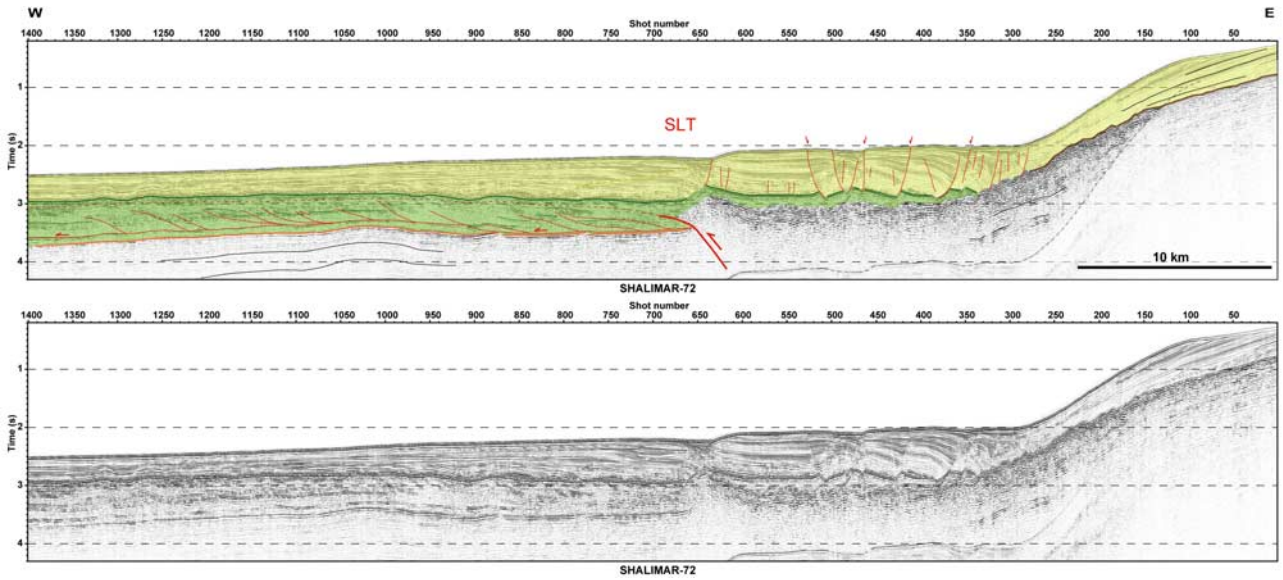

Figure 5. Profile HS-72 in southern offshore area. SLT, South Lebanon thrust zone.

Mart and Ryan, 2007]. Gravity-driven extensional spreading above a ductile evaporite layer usually generates tilted blocks, grabens and rollover systems. On profile HR-126, the fault at SP 280 for instance, with its curved shape and downdip increase in hanging wall dips and offsets, is typical of a rollover.

[19] Profile HS-72 (Figure 5) coincides roughly with high-resolution profile HR-126 (Figure 4) but extends much farther into the basin. While the shallow structure east of SP 500 is best imaged on the high-resolution data, the high-speed data reveal strong reflectivity for about 300 ms beneath the base of the Messinian, implying a different depositional environment at the beginning of the Messinian dessication event. Around SP 630, a N–S trending, elongated surface channel is bounded on its east side by a surface scarp and a west dipping normal fault in the turbidites. The evaporite layer underneath is clearly deformed: it is uplifted and thinned by a factor of three on the landward relative to the seaward side, and is also tilted landward (between SP 600–640). Miocene beds under the evaporites (between SP 590–640) appear to be folded. Neither the tilt that accompanies the uplift of the evaporites nor the folding of Miocene sediments can be accounted for with motion on the shallow normal fault only. The entire structure is fully explained, on the other hand, if the underlying structure is a blind thrust ramp that bends into a flat décollement level at the base of the salt. The normal fault in the turbidites above may be interpreted as an accommodation fault absorbing extension at the hinge of the ramp anticline, above the ramp to flat bend [see also *Elias*, 2006; A. Elias et al., manuscript in preparation, 2009]. Between SP 660 and 790, a sand wave is imaged within the upper turbidites. Between SP 920 and 1090, the base of the Messinian and underlying strata are again gently folded, but neither the top of the Messinian nor the seafloor are, which implies shortening prior to ~5 Ma. Within the Messinian, which thickens slightly seaward, there are flat-lying or east dipping reflectors that may be interpreted as imbricates or even duplexes on multiple small thrusts rooting into a décollement near the base of the Messinian.

[20] Profile HS-76b (Figure 6) is the southernmost long NW–SE profile in the survey area. In the eastern half of the

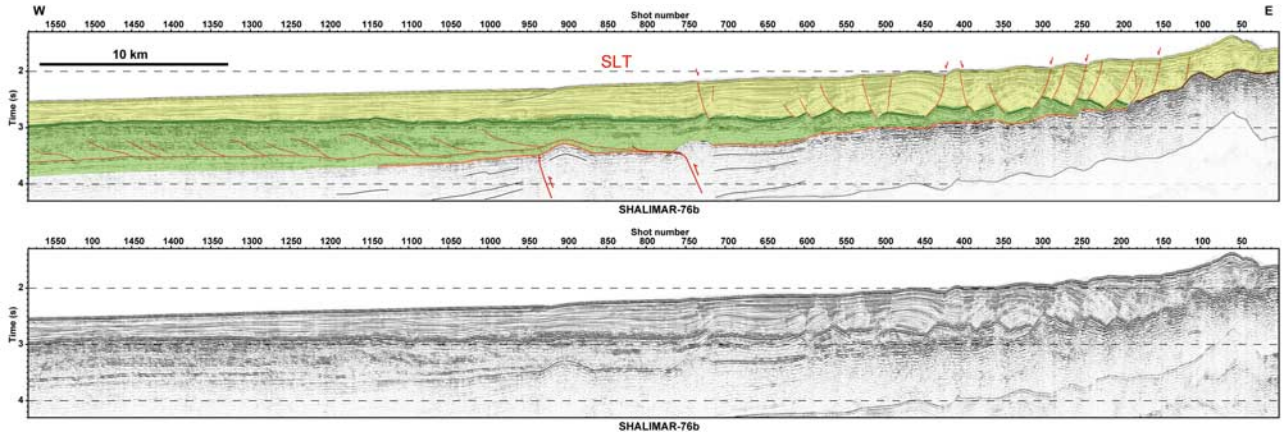

Figure 6. Profile HS-76b in southern offshore area.

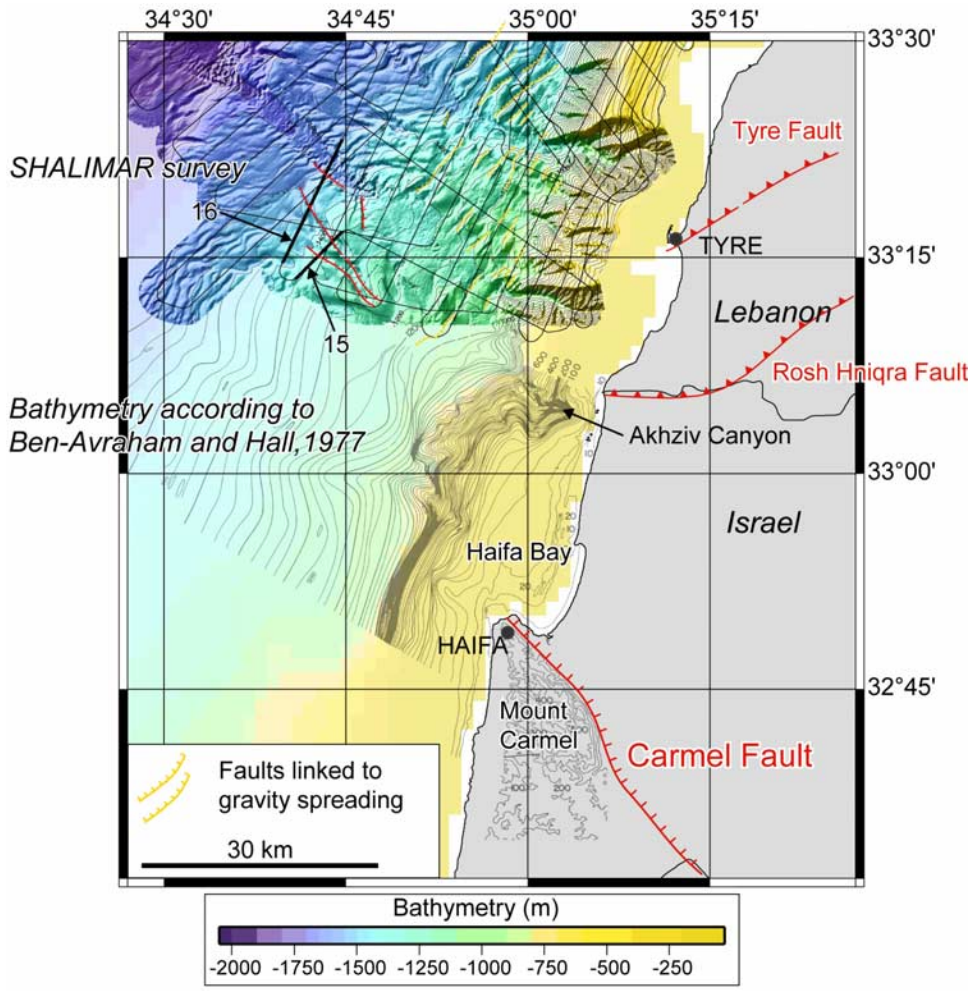

Figure 7. Map of southern Lebanon and northern Israel offshore area. Bathymetry is from Shalimar survey. Contours in southern half are from survey conducted by *Ben-Avraham and Hall* [1977] offshore of Haifa. Trace of NW trending Carmel fault on land is marked in red, as well as subparallel normal fault scarps detected in Shalimar bathymetry. Faults related to gravity spreading (salt tectonics) mapped in southern Lebanese offshore area are marked in yellow. Other active faults are in red.

profile, the deformation pattern of the evaporites and overlying turbidites is similar to that described above. Salt tectonics is expressed through a series of listric normal faults that affect a wider area than on profile HS-72 (Figure 5). Both east and west dipping faults are imaged, but mostly west dipping ones reach the surface. The associated fault scarps are clearly identifiable in the bathymetric data, but they are usually too short (a few kilometers in length) to be followed from one profile to the next. Rollover and turtleback structures [e.g., *Vendeville and Cobbold*, 1987] are observed in the turbidites, indicative of gravity spreading. The base of the Messinian and underlying sediments are folded at two locations, between SP 720 and 770 and between 870 and 930, again without any associated deformation of the top of the Messinian and seafloor. Both anticlines appear to have grown on top of blind thrust faults that can be traced within the pre-Messinian Miocene beds. The easternmost anticline seems to be the southward continuation of that imaged farther north on profile HS-72. Seaward, the evaporite layer also shows internal structuring, most likely by imbricates and duplexes.

[21] At the southern extremity of the survey area, NW trending normal fault scarps roughly aligned with the NE dipping Carmel fault are observed in the bathymetry. They correspond to steeply dipping normal faults on several seismic profiles (Figure 7). A short section of profile HS-15 (Figure 8a) for instance displays NE dipping normal faults affecting the turbidite layer (up to 800 ms thick), the evaporite layer (about 400 ms thick) and the pre-Messinian "basement," with clear offsets of the top and base of the Messinian. The blocks between the faults are tilted southwestward. Two of the faults reach the surface at SP 830 and 750. Profile HS-16 (Figure 8b), located about 5 km to the NW, shows similarly deep-rooted normal faulting, with faults reaching the surface at SP 190, 300, and 340. Both the Messinian and the sediments underneath also show normal faulting and block tilting. Eleven profiles subsequently shot to the northwest indicate, however, that this active normal fault zone, which keeps striking roughly perpendicular to the thrusts documented above and clearly reaches deeper than the base of the Messinian, does not continue farther NW into the Levant basin.

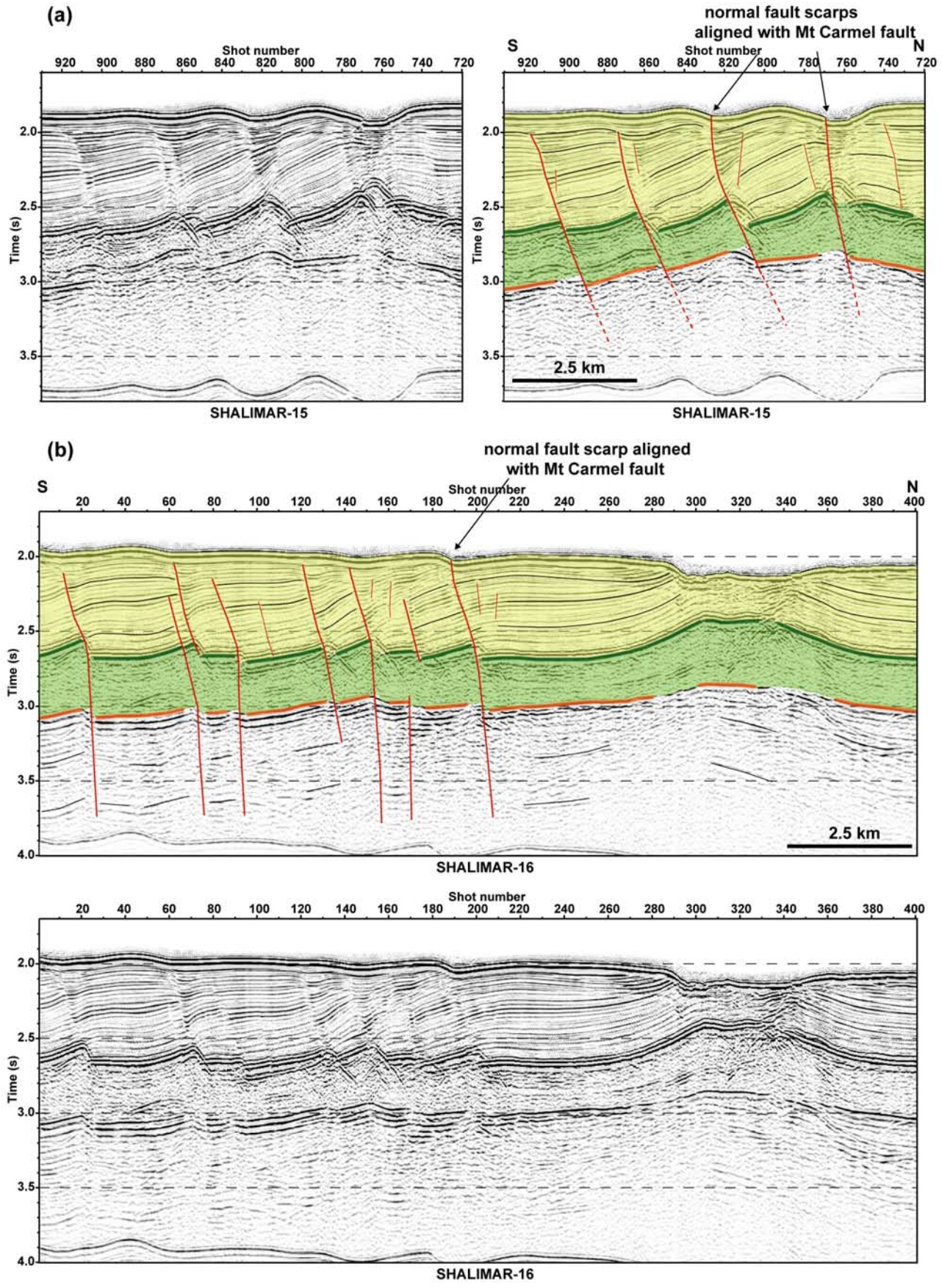

Figure 8. Crops from high-speed profiles in southern offshore area: (a) profile HS-15 and (b) profile HS-16.

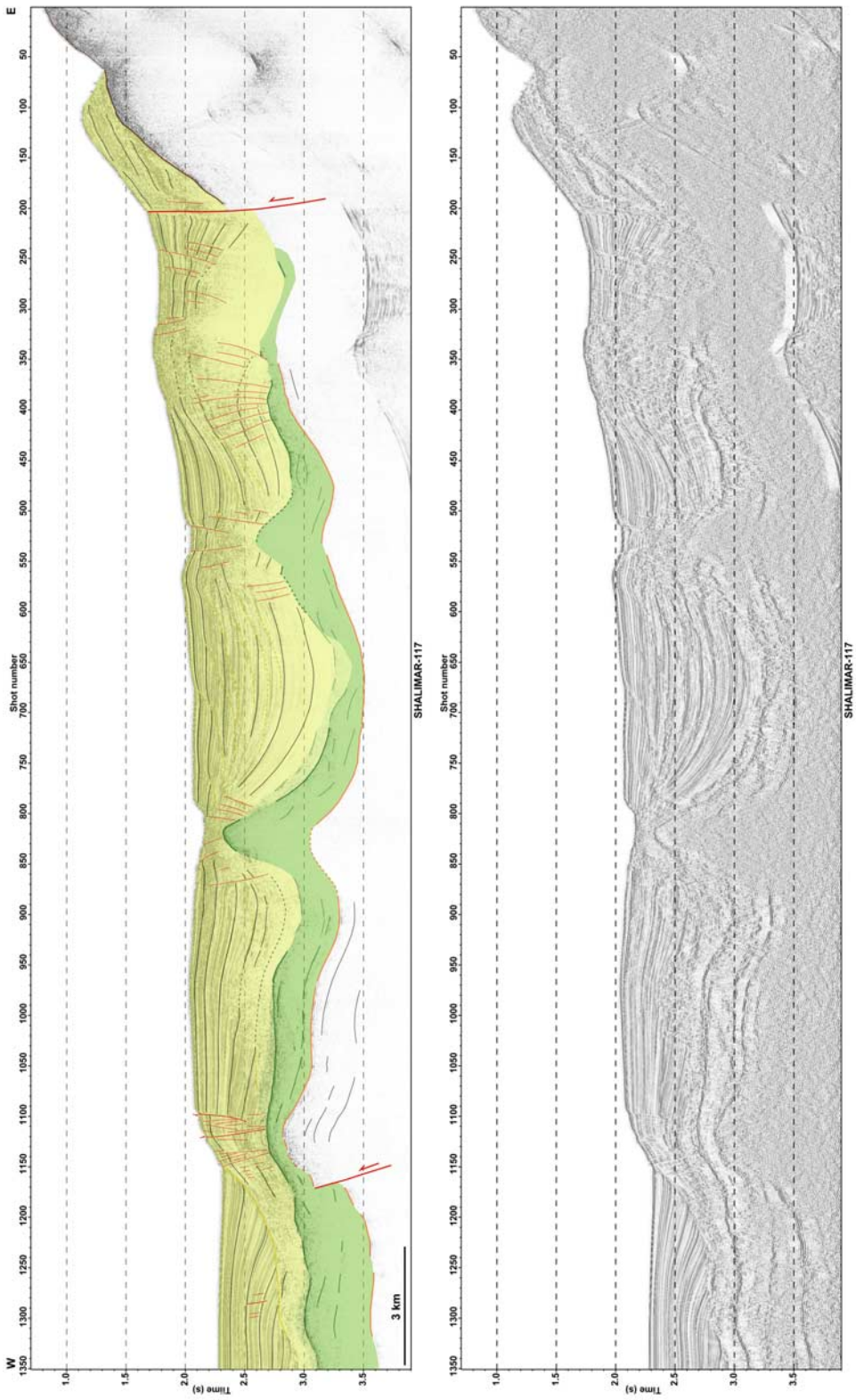

Figure 9. Profile HR-117 in central offshore area.

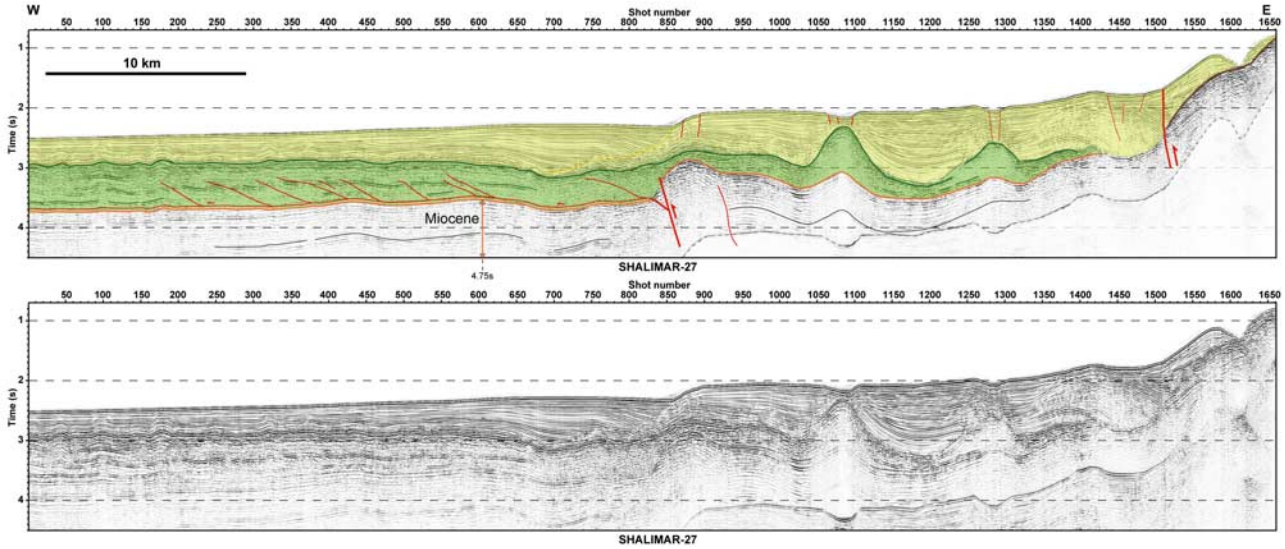

Figure 10. Profile HS-27 in central offshore area.

5.3. Central Offshore Area (Beirut-Byblos)

[22] Profile HR-117 (Figure 9) runs perpendicular to the coast west of Jounieh and samples one of the most deformed zones. The base of the continental slope (SP 200) is marked by a clear break in seafloor topography, associated with the presence of steep faults. Fanning of Plio-Quaternary sediments suggests normal motion at shallow depth. Deeper down, the turbidite beds curve upward against the main fault. The MES, which is steeper in the central offshore area than anywhere else along the margin, is truncated and displaced vertically (with an offset of ~220 ms) by this fault, which therefore brings Cretaceous beds onto Plio-Quaternary turbidites. Furthermore, the surface expression of the fault on the deep-towed side-scan sonar data is that of a thrust fault scarp [*Elias et al.*, 2007]. We thus interpret the main fault at SP 200 as a deep thrust ramp. Just to the west, between SP 240 and 480, the Messinian layer terminates as a thin, contorted lens, apparently above a deep anticline. The turbidites immediately above are affected by normal faults with small offsets. Farther westward, the profile cuts across two diapiric ridges that culminate at SP 530 and SP 820. In the westernmost diapir, the M reflector rises to 2.35 s bsl, with a maximum evaporite thickness of 750 ms. Both diapir apexes are overlain by thin turbidites, on top of which lie channels (at 35°23′E and 35°27′E) bounded by small normal faults. In between the two diapirs, which are 7.5 km apart, thick turbidite deposits (up to 2.2 s) are found in broad synclines. In the depth domain, that is, after taking into account the stretch effect produced by the high-velocity evaporites, the base of the diapirs probably displays relatively flat topography, as discussed in the next section. Farther west however, between SP 900–1170, both the base of the Messinian and reflectors underneath are clearly folded (and would remain so if the section were converted to depth), with a blind thrust ramp displacing the base of the Messinian at SP 1170. The evaporite layer thickens abruptly by a factor of ~4 across this fault. Above the folded Tortonian beds, the evaporites thickness is only 130 ms, and steep normal faults accommodate active hinge extension within the turbidites. We interpret the structure between SP 1050–1250 as a ramp anticline, similar to but more beautifully expressed than the one previously identified on profile HS-72 (Figure 5). At the front of the anticline (SP 1150; 34°18′E, 35°18′E), a feature that resembles a shallow-dipping growth fault (Figure 5, in yellow) bounds east dipping turbidites that fan downward. Note again that shallow, active normal faulting (here chiefly the steep normal faults found only at the top of the anticline) cannot be interpreted independently from observations of shortening (presence of a bathymetric ridge marked NR in Figure 2, folded base of the Messinian layer and older rocks underneath, and faulted base of the Messinian). The above interpretation of a ramp anticline, implying tectonic shortening, is the only one capable of simultaneously explaining all the observations of recent and active deformation provided by the seismic data.

[23] Profile HS-27 (Figure 10), the high-speed equivalent of profile HR-117, extends farther into the basin. West of the frontal anticline described above, about 30 km from shore, this profile shows landward dipping reflectors within the evaporite layer, which likely correspond to imbricates or duplexes, with small thrusts rooting into a décollement near the base of the salt. These features extend at least as far as 55 km from shore and therefore must absorb a significant fraction of the total shortening. Our sections are unfortunately not long enough to determine the outer limit of this deformed zone, or whether a roof décollement on top of the evaporites actually exists and ultimately ramps upward to the seafloor.

[24] Profile HR-102 (Figure 11) runs offshore of Beirut, about 15 km south of profile HR-117. In the western half of the profile, the base of the Messinian is clearly folded around SP 520–770 and SP 130–300, with east dipping thrust ramps cutting the Miocene underneath the west facing limbs of both anticlines, but the deformation of the overlying Messinian layer and Plio-Quaternary sequence differs from that seen on profile HR-117. The first anticline to the east is associated with a rise of the Messinian layer, and a broad channel incises the top of the turbidites. On top of the second there is little deformation of reflector M but asymmetric warping of the thick turbidites above it has created

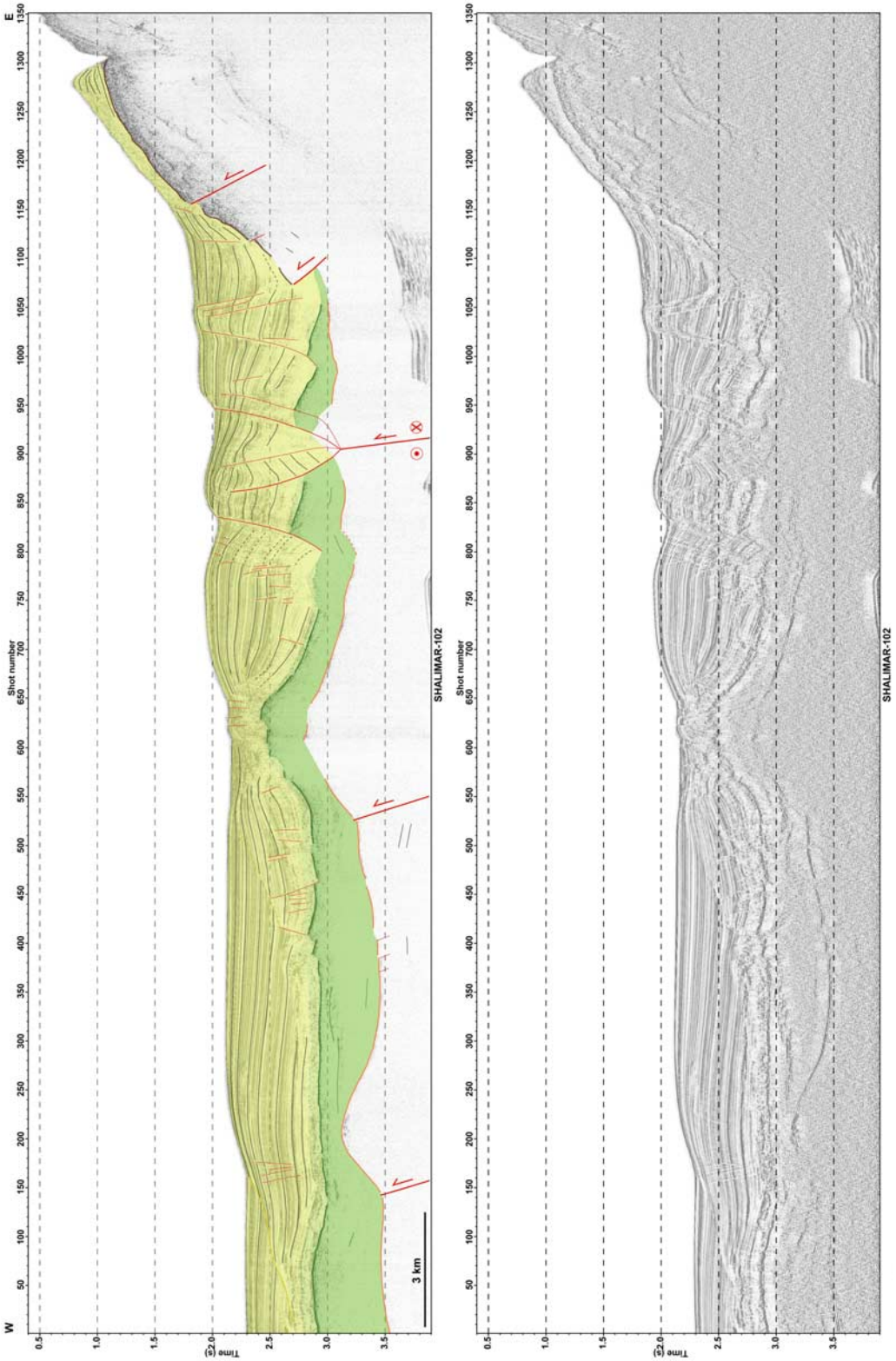

Figure 11. Profile HR-102 in central offshore area.

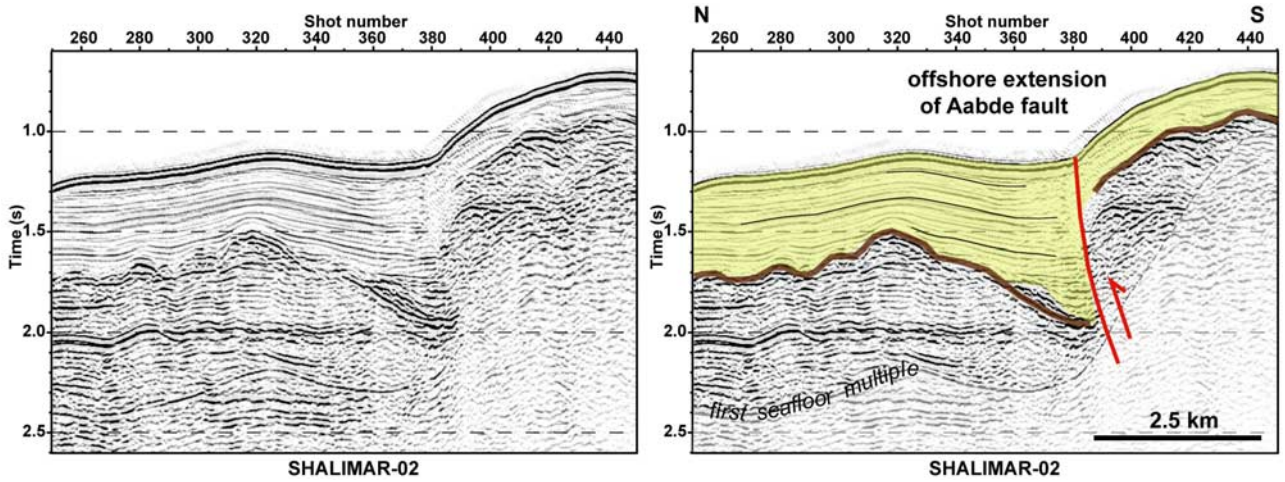

Figure 12. Crop from profile HS-02 in transition zone between northern and central offshore areas.

clear a NE–SW trending, west facing bathymetric scarp about 11 km long. Overall, this frontal anticline (whose bathymetric expression is marked as SR in Figure 2) is smoother and less developed than that on profile HR-117 (whose bathymetric expression is marked as NR in Figure 2). The MES is well imaged near the eastern end of the profile, with a possible east dipping thrust fault cutting through the steeper part of the MES at SP 1160. Another, larger thrust may have uplifted the downdip termination of the MES relative to the evaporites pinch-out at about SP 1100. While the fault planes themselves are not imaged in the seismic data (e.g., as high-amplitude reflectors), the proposed interpretation of thrusts penetrating pre-Messinian sediments and producing vertical offsets in the MES is the most plausible. Between SP 800 and1100, the top and base of the Messinian are deformed, with a systematic eastward tilt of the M reflector. Several listric normal faults, with either landward or seaward dips, are imaged within the turbidites, and channels have localized along the seafloor cumulative scarps created by two of them at SP 960 and 830. These faults also offset M and may root into the evaporites. This pattern of deformation can be interpreted either as the expression of salt tectonics, or as a consequence of a lateral component of slip on deep, oblique thrust ramps.

5.4. Transition Between the Northern and Central Offshore Areas (Byblos-Tripoli)

[25] A short section of profile HS-02 offshore of Tripoli (Figure 12), which strikes N–S, shows a clear footwall wedge underthrust, with Miocene rocks emplaced above the Plio-Quaternary turbidites, demonstrating the existence of a steep south dipping thrust fault. The fault trace corresponds

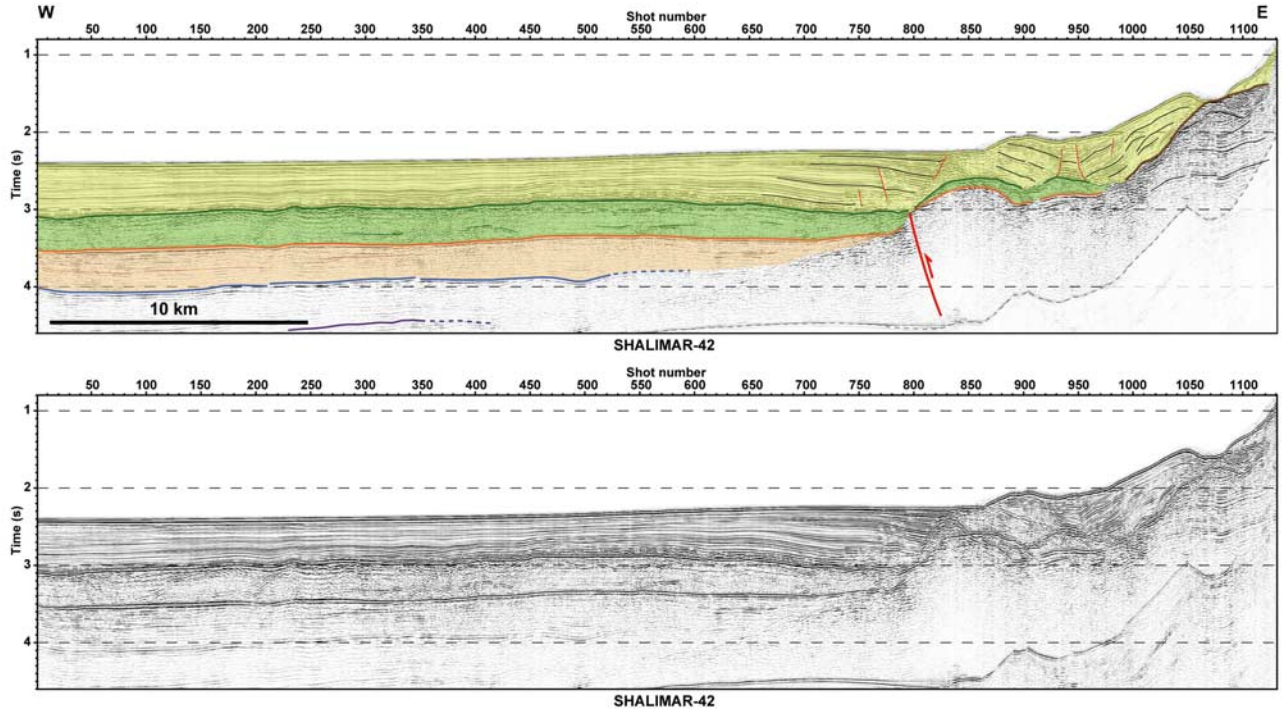

Figure 13. Profile HS-42 in transition zone between northern and central offshore areas.

to a rather steep bathymetric gradient around 34°30′N, also imaged on three other seismic profiles. We interpret this fault as the continuation at sea of the Aabde-Rankine fault, which is responsible for the uplift of the Rankine Islands offshore of Tripoli. This fault, with combined strike-slip and thrust motion, likely acts as the northernmost lateral ramp of the offshore thrust system [see also *Elias*, 2006; A. Elias et al., manuscript in preparation, 2009]. It does not seem to continue seaward west of 34°29′N, 35°34′E.

[26] Comparison between profile HS-42 (Figure 13) and the undeformed, reference profile HS-50 (Figure 3) highlights the type of deformation occurring offshore of Batroun and Enfeh. Instead of pinching out at the base of the slope, the evaporites are now interrupted, with an elongated, uplifted and contorted body on the landward side (between SP 830–980), separated from the bulk of the relatively undisturbed and flat evaporitic layer in the basin. The latter appears to be truncated, at SP 800, by the seaward dipping limb of a large anticline, likely growing above an east dipping thrust fault, on the back limb of which lies the evaporite lens. Above this lens, the Plio-Quaternary sediments, instead of being only gently seaward dipping as on profile HS-50, are cut by normal faults that define either east or west dipping blocks. At the front of the fold, the Plio-Quaternary sequence thickens with clear landward dipping reflectors that appear to terminate against west dipping normal faults (although the image is locally complicated by the presence of possible side swipes). Such a folding pattern (with thinning and uplifting of the evaporites above the hinge of a growing anticline, and thickening of the Plio-Quaternary cover at its front with an interplay between blind thrust and normal faulting) is similar to that observed on profile HS-72 (Figure 5) in the southern offshore domain, and on profiles HS-27 and HR-117 (Figures 9 and 10) in the central offshore domain. Farther north, bathymetric data show that the anticline imaged on profile HS-42 emerges above the surrounding seafloor, while another HR seismic profile (not shown here) images a layer of Plio-Quaternary sediments directly capping the MES, indicating that this particular anticline stood above the sea surface during the Messinian salinity crisis.

[27] Profile HR-107 (Figure 14), also offshore of Batroun/Enfeh, was shot at an angle to profile HS-42 (Figure 13). It shows very clear evidence of folding and thrusting of the base of the Messinian and underlying Miocene reflectors. The Messinian layer is divided into three slices, all of them uplifted and tilted landward, which cap west facing anticlines growing on blind, east dipping thrust faults (such as imaged at SP 200 and SP 450). Above M, the Plio-Quaternary layer shows large variations in thickness and is affected by small normal faults, three of them reaching the surface at SP 220, 450 and 490; the faults at SP 450 and 490 bound a channel. Farther east, two more thrust faults are observed, the first one at the easternmost tip of the evaporites at SP 570, cutting clearly through the overlying turbidites and the second one offsetting the MES around SP 730.

5.5. Transition Between the Southern and Central Offshore Areas (Beirut-Saida)

[28] South of Beirut, profile HR-121 (Figure 15) shows a steep slope break at SP 670, where the Plio-Quaternary cover is locally interrupted and the MES emerges at the seafloor. This slope break is probably associated with the presence of an east dipping thrust fault. Farther landward, east dipping, folded beds and thrust imbricates below the MES, likely of Cretaceous to lower Miocene age, are unconformably capped by layers of gently west dipping turbidites. At SP 750, another west dipping thrust fault truncates the MES and the evaporites pinch-out continuing above into the thick turbidites. This pattern (steep slope break, steep MES, discontinuous turbiditic deposits, accumulation of turbidites at the base of the slope) contrasts markedly with that observed on profile HR-126 (Figure 4), where there is little evidence for thrust faulting at the corresponding location, if any. West of the termination of the MES, an elongated, evaporitic body is tilted landward and imbricated by one thrust while being separated from the rest of the evaporite layer in the basin by yet another, very steep fault. Although here the data penetration does not allow to image reflectors well below the evaporite lens, this is suggestive of transpressional faulting and folding at the base of the slope (between SP 900 and 760). Farther west, the base of the Messinian is folded (SP 1210–1000), likely with additional transpressional movement, along the Saida fault zone (fault at SP 1040). The Plio-Quaternary sequence is clearly affected by gravity spreading, with a number of normal faults, including one large listric fault with a rollover at SP 1040, rooting at the top of the evaporites, and bounding and dissecting mostly east dipping and drag-warped turbidite layers.

[29] Profile HS-62 (Figure 16) is one of six profiles shot to investigate a potential offshore extension of the Roum fault (in fact the Saida fault). It runs perpendicular to the approximately north–south striking fault trace seen in the bathymetry, which continues along a N–S trending canyon just west of Saida. As on profile HR-121, the MES is covered by a thick turbidite layer (up to 650 ms thick) on the plateau, then dips steeply and is overlain by a much thinner sequence (100 ms) on the slope. The landward pinch-out of the evaporites (SP 290–240) is relatively complex, likely owing to the passage of the transpressional Saida fault around SP 235. Farther west, a large normal fault bounding east dipping turbidites and rooting at the base of the evaporites reaches the seabed along a small channel at SP 415. Immediately underneath the footwall, the evaporites reach a thickness of 600 ms.

6. Isopach Maps

6.1. Preparation of the Maps and the Question of Seismic Velocities

[30] Horizon picks in two-way travel time for the seafloor, the M and N reflectors and the MES surface were gridded at ~200-m spacing within an oblique rectangular box oriented N26°E encompassing the Shalimar survey area. This ensured that structures oriented roughly parallel to the coast would be adequately mapped.

[31] The main problem is to determine the exact values of interval velocities that should be used to depth-convert these time domain offshore maps of the above reflectors. The short-streamer data collected during the survey are insufficient to pick reliable stacking velocities because only the nearest part of the normal move out hyperbola is sampled.

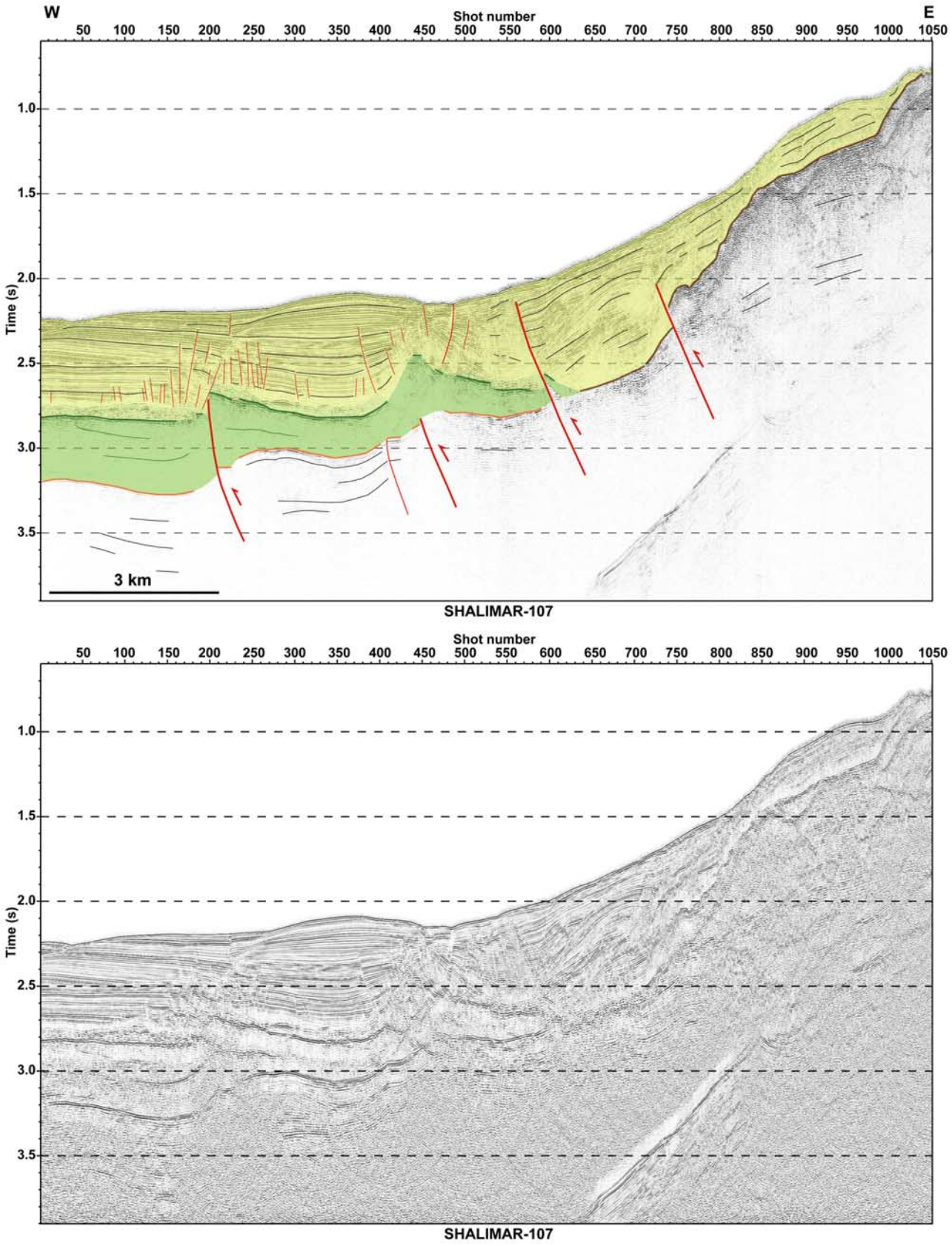

Figure 14. Profile HR-107 in transition zone between northern and central offshore areas.

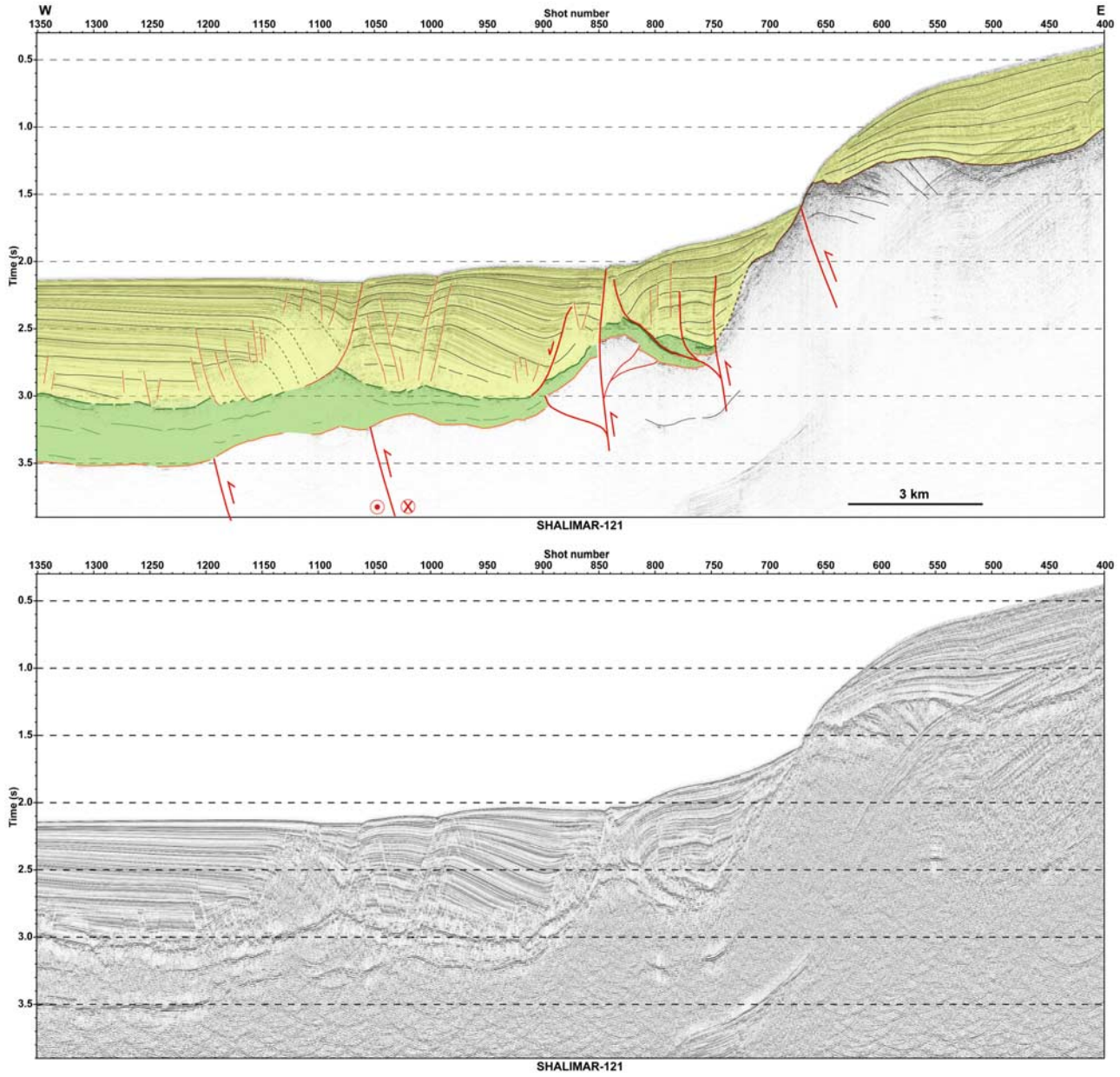

Figure 15. Profile HR-121 in transition zone between central and southern offshore areas.

From migration velocity analysis, velocity values found for Plio-Quaternary sediments in neighboring areas of the Levant basin are 2–2.5 km/s [*Vidal et al.*, 2000]. They are 2 km/s from exploration well data offshore of Israel [*Bertoni and Cartwright*, 2006]. Other authors adopt lower values for their depth conversions (1.9 km/s in the work of *Ben-Avraham et al.* [2006] and 1.7 km/s in the work of *Hall et al.* [2005]), without providing further justifications. Besides, the topmost deposits are probably saturated with seawater, and the sediments become more compacted and denser at depth. This implies a downward velocity increase, and hence taking into account velocity variations within the Plio-Quaternary layer would be necessary to achieve proper depth conversion. The conversion problem is rendered particularly difficult by the presence of the evaporite layer. Since the evaporite velocity is high, a given difference in velocity would translate into a larger error in depth than within the Plio-Quaternary unit. A review of the literature for neighboring areas yields the following evaporites velocity values: 4.2 km/s from modeling of large refraction lines [*Ben-Avraham et al.*, 2002; *Netzeband et al.*, 2006a], 4.3–4.5 km/s from migration velocity analysis [*Vidal et al.*, 2000], and 3.5–4.5 km/s from exploration well data offshore of Israel [*Bertoni and Cartwright*, 2006]. Depth conversion using a value of 4.5 km/s produces severe plunging of the N horizon beneath the largest diapirs, instead of the expected uplift or flattening. To a first order, such a plunging shape appears to be implausible (Figure 17). In fact, there are reasons why the evaporite layer offshore of Lebanon might have lower interval velocity values compared to other sites in the Levant basin, far offshore of Israel or SE of Cyprus. The high, mountainous Lebanese margin is deeply incised by numerous fluvial canyons with steep downstream profiles. During the Messinian salinity crisis,

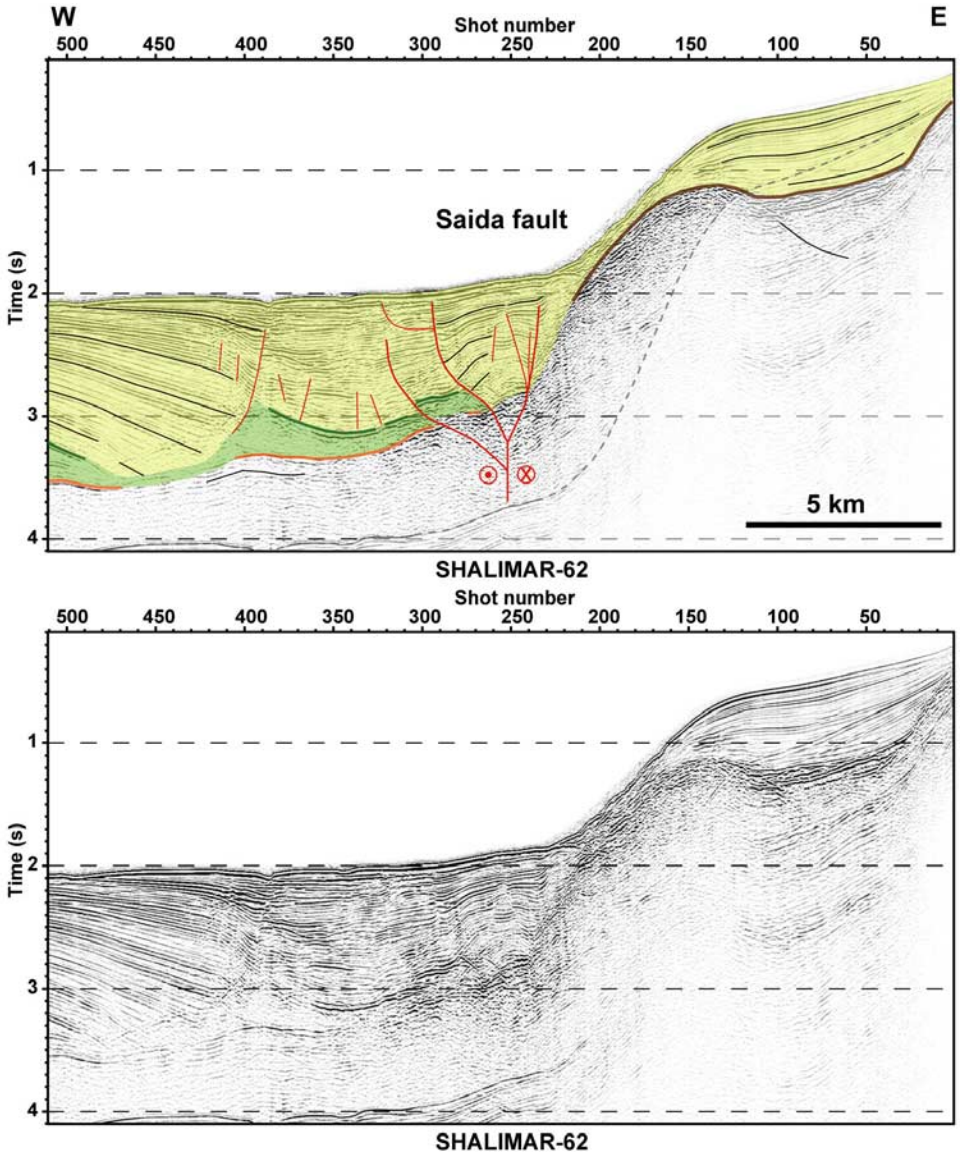

Figure 16. Profile HS-62 in transition zone between central and southern offshore areas.

these canyons must have provided abundant detritic material that fanned into the evaporites, hence yielding a lower interval velocity. Even if the Messinian layer is depth converted with a velocity of 3.8 km/s, however, the peculiar, convex-downward bowl shape of the N horizon remains. This highlights the difficulty there is to provide accurate depth values and thicknesses when no within-site velocity estimates are available, which could be obtained either from drilling or multichannel seismics with sufficiently long offsets. Consequently, the isopach maps presented in sections 6.2 and 6.3 are plotted for now in ms two-way travel time.

6.2. Plio-Quaternary Turbidites Thickness Map

[32] This map (Figure 18) represents the "thickness" of the post-Messinian deposits above the M horizon in deep water and the MES on the slope and platform. Results show that Pliocene and Quaternary deposits are 400–500 ms "thick" in the abyssal plain of the Levant basin, which would correspond to an actual thickness of 320–550 m with velocities of 1.6–2.2 km/s. Closer to shore, very little recent deposition occurred in the canyons incising the continental slope (where the erosional surface often crops out) while thicker deposits are found on plateau areas where the shelf is large (e.g., south of Beirut, with up to 700 ms). In deeper water, the water depth varies much less and much more smoothly than does the depth of the M horizon, and hence the thickness map essentially reproduces the behavior of the M horizon, which translates into strong thinning of the turbidite layer above the evaporite diapir walls and thick accumulation into broad troughs in between. Areas with more than 800 ms of Plio-Quaternary sediments are observed within 35–45 km from the coast, with two maxima, one halfway between Beirut and Saida (1.4 s, i.e., 1100- to 1500-m thickness, 25 km from the coast), and the other between Byblos and Jounieh (1.2 s, i.e., 960- to 1320-m thickness, 20 km from the coast). In addition to the short-wavelength, tectonic variations in thickness near the margin, the map shows quite clearly the overall seaward thinning of the Plio-Quaternary sediment apron toward the Levant abyssal plain.

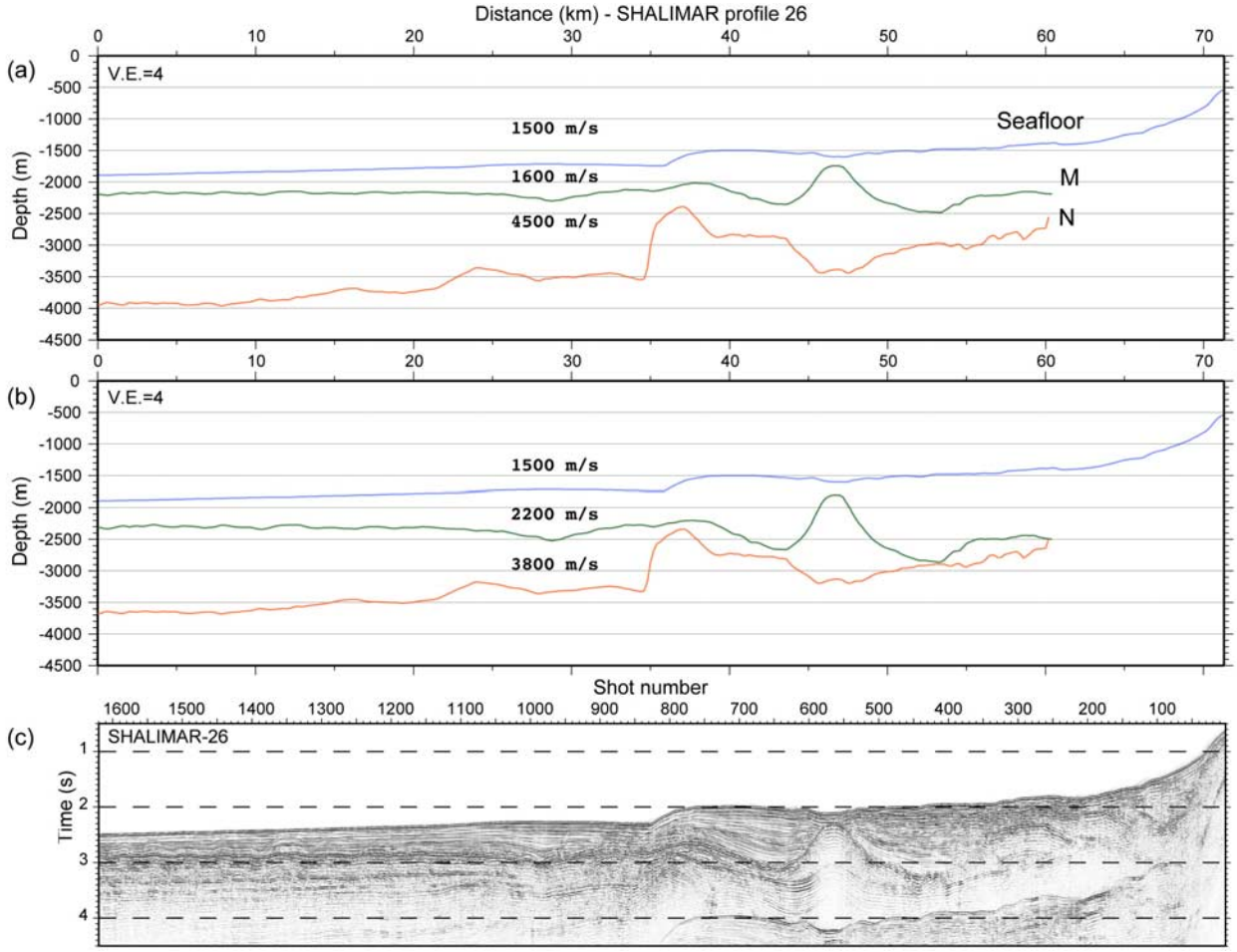

Figure 17. Tests of depth conversion of several interfaces (M and N horizons) on (c) profile HS-26, with constant velocities of (a) 1.6 and 4.5 km/s and (b) 2.2 and 3.8 km/s, for Plio-Quaternary and Messinian layers, respectively.

[33] Turbidites from the Nile delta have been identified as the major source of Plio-Quaternary deposits in the southern Levant basin, and the Nile turbidites are known to extend farther north, in particular, offshore of Israel [*Garfunkel and Almagor*, 1985]. Here by contrast, the occurrence of thicker Plio-Quaternary deposits just along the base of the margin in the central Lebanese offshore area implies rapid sedimentation derived from a local source. Turbidite channels connected to large onshore river canyons carrying the erosion debris of the Mount Lebanon range are well imaged in the seafloor bathymetry and backscatter imagery data [*Elias*, 2006; A. Elias et al., manuscript in preparation, 2009]. The proximity of the Lebanese ranges and the presence of such channels suggest that most of the Plio-Quaternary deposits offshore of Lebanon have been fed by turbidite avalanches resulting from the erosion of the mountains, the growing relief and associated seafloor subsidence.

6.3. Messinian Evaporite Thickness Map

[34] The maximum evaporite thickness observed within the Shalimar survey area is about 900 ms, that is, 1800 m assuming an average velocity of 4 km/s, WNW of Saida, about 71 km offshore from the coast (Figure 19). Offshore of Israel, comparable evaporite thicknesses are observed much farther seaward, ~120 km from the coast, between Tel-Aviv and Haifa [*Bertoni and Cartwright*, 2006]. South of Beirut, the gradient reflected by the spacing between adjacent isocontour lines tends to increase northward, bringing thick evaporites even closer to the shore. Similarly, the 200-ms contour line is much closer to shore in the central offshore area (11–15 km) than it is in the southern offshore area (26–30 km). The Messinian deposit distribution thus also reflects the narrowing and steepening of the continental margin between northern Israel and Mount Lebanon. Overall, a clear seaward thickening of the Messinian unit is observed in the Shalimar survey area, similar to that offshore of Israel, but with two notable exceptions. In the northwest, two submarine thrust ridges mark the deformation front of the Cyprus arc, along which the Sinai microplate subducts beneath Anatolia. The evaporites pinch out along either limb of the westernmost ridge (Latakia), which indicates that its top was emerged during the Messinian. Owing to the subduction-related, tectonic shrinking of the Levant basin, the maximum offshore evaporite thickness between the two Cyprus ridges and the Lebanese margin north of Tripoli is only about 500 ms. In addition, the central Lebanese Beirut-Batroun offshore area displays a complex pattern with NNE–SSW trending thick evaporite

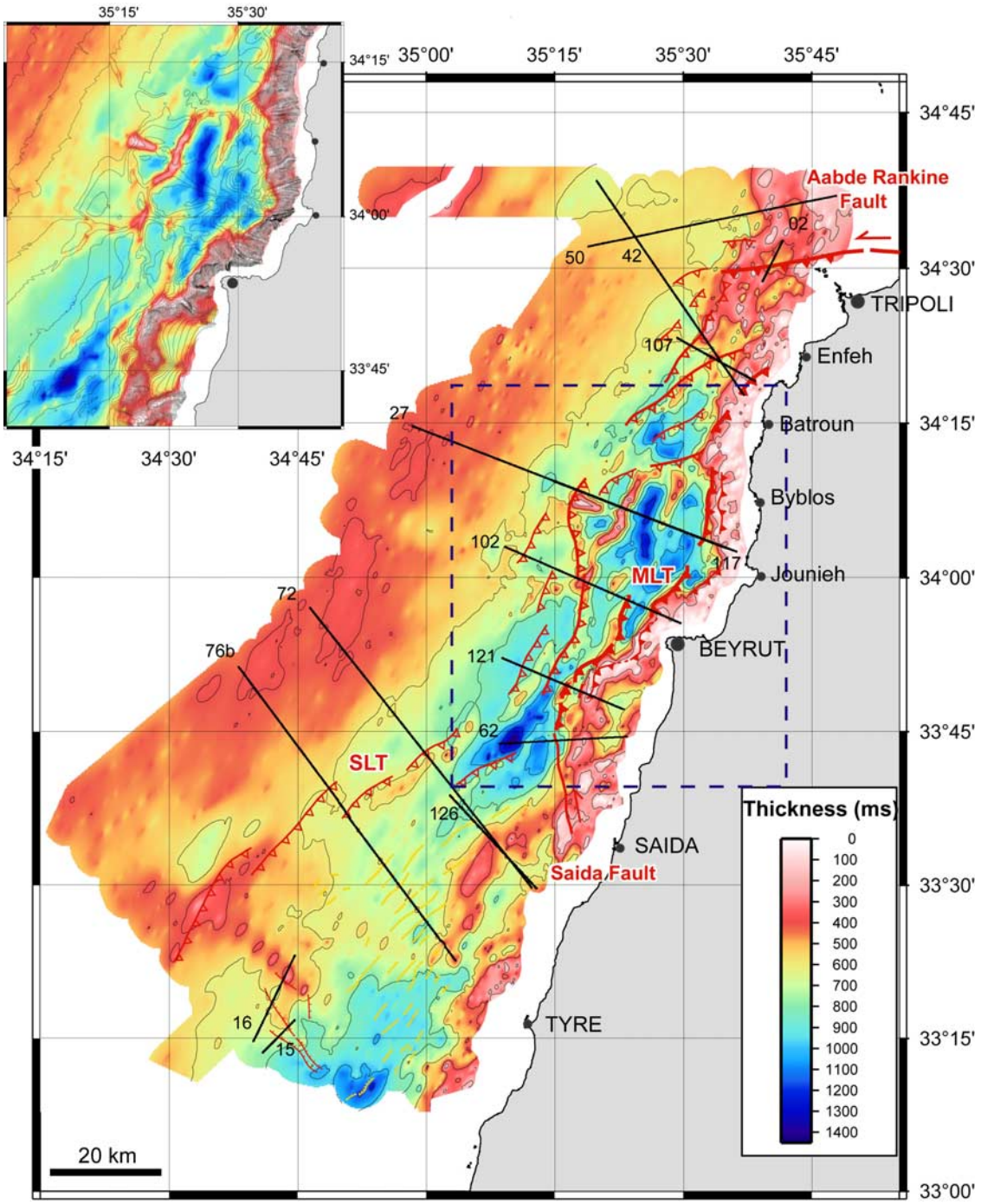

Figure 18. Plio-Quaternary turbidite thickness map, gridded at ~200-m spacing within an oblique rectangular box oriented N26°E (parallel to margin) encompassing Shalimar survey area. Thickness is expressed in milliseconds two-way travel time (ms), with contours every 200 ms. Faults are modified after *Elias et al.* [2007]. Inset shows same thickness map for central offshore area, overlying 50-m bathymetric contours instead. MLT, Mount Lebanon Thrust.

zones alternating with zones where the evaporite layer becomes very thin. Two such zones are the elongated diapiric belts (salt walls) mapped offshore of Byblos and Jounieh (16 km long in the west one and 10–12 km long in the east, respectively). Their widths range between 2.2 and 2.9 km. The linearity of such structures is consistent with a tectonically controlled origin along the hinges of anticlines. Other salt domes are also present offshore of Jounieh and Batroun. Areas with very thin evaporites are found along the pinch-out wedge of the evaporite layer at the base of the slope along the entire survey area. The other areas with thin evaporites lie along the crest of several anticlines, such as those that mark the outer edge of the Jounieh plateau (cf profiles HR-117 and HR-102, but also HR-121, HS-42, and HS-72) and result from strong uplift (in time) of the base of

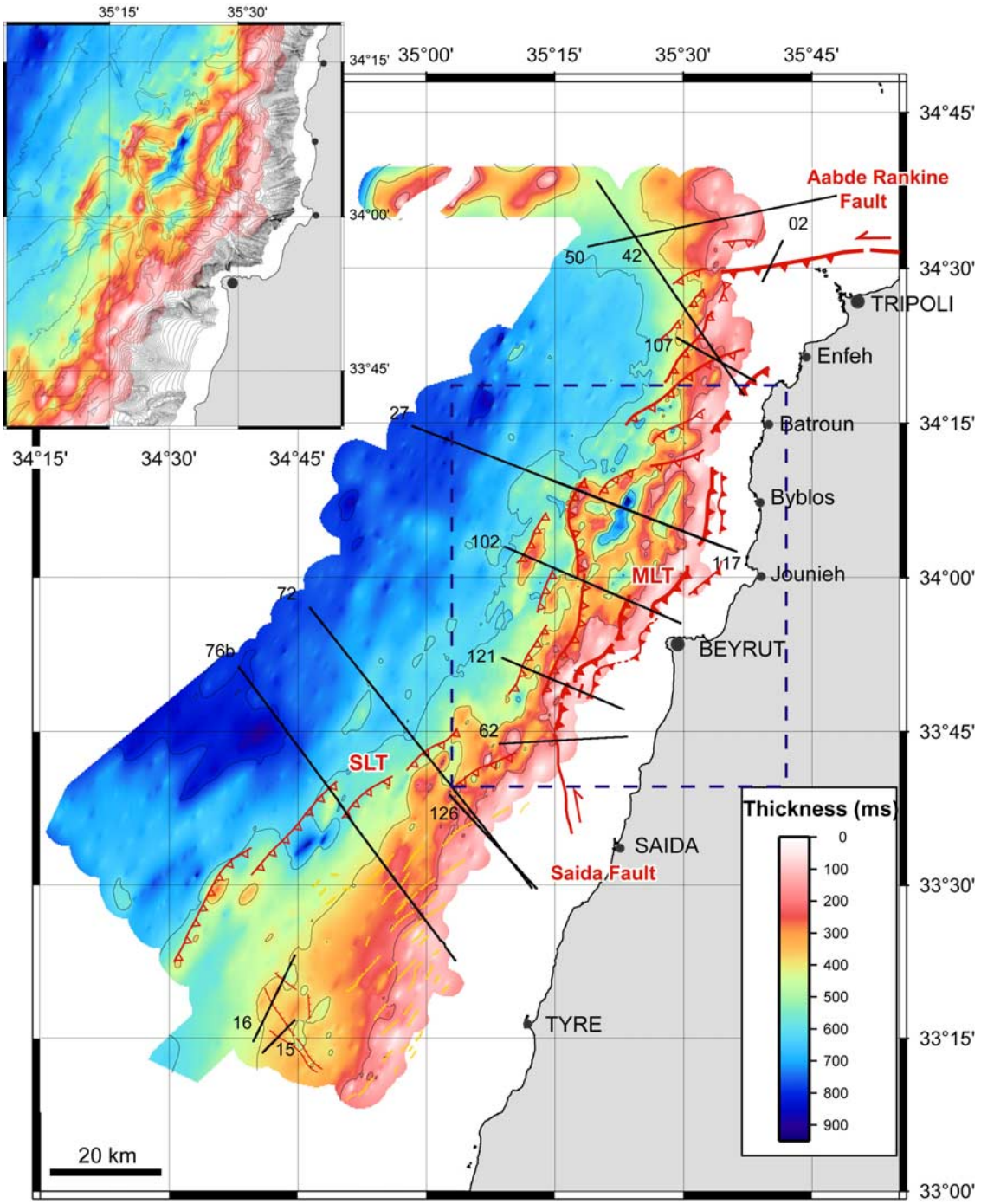

Figure 19. Messinian evaporites thickness map, gridded at ~200-m spacing within oblique rectangular box oriented N26°E (parallel to margin) encompassing Shalimar survey area. Thickness is expressed in milliseconds two-way travel time (ms), with contours every 200 ms. Faults are modified after *Elias et al.* [2007]. Inset shows same thickness map for central offshore area, overlying 50-m bathymetric contours instead.

the Messinian with much less uplift of the top, suggestive of salt thinning during anticlinal growth.

7. Summary, Discussion, and Conclusion

7.1. Mount Lebanon Offshore Thrust System

[35] The Shalimar data establish the presence of a ~90-km-long, ~30-km-wide submarine fold-and-thrust belt just offshore of the broadest and highest part of the Mount Lebanon ranges [see also *Elias*, 2006]. The belt also faces the part of the shoreline (i.e., between Beirut and Tripoli) that displays the most prominent active uplift, as documented by numerous abandoned marine-cut terraces and bioconstructional platforms [*Sanlaville*, 1977; *Morhange et al.*, 2006; *Elias et al.*, 2007]. This offshore area of recent and ongoing shortening is limited to the north by the Aabde

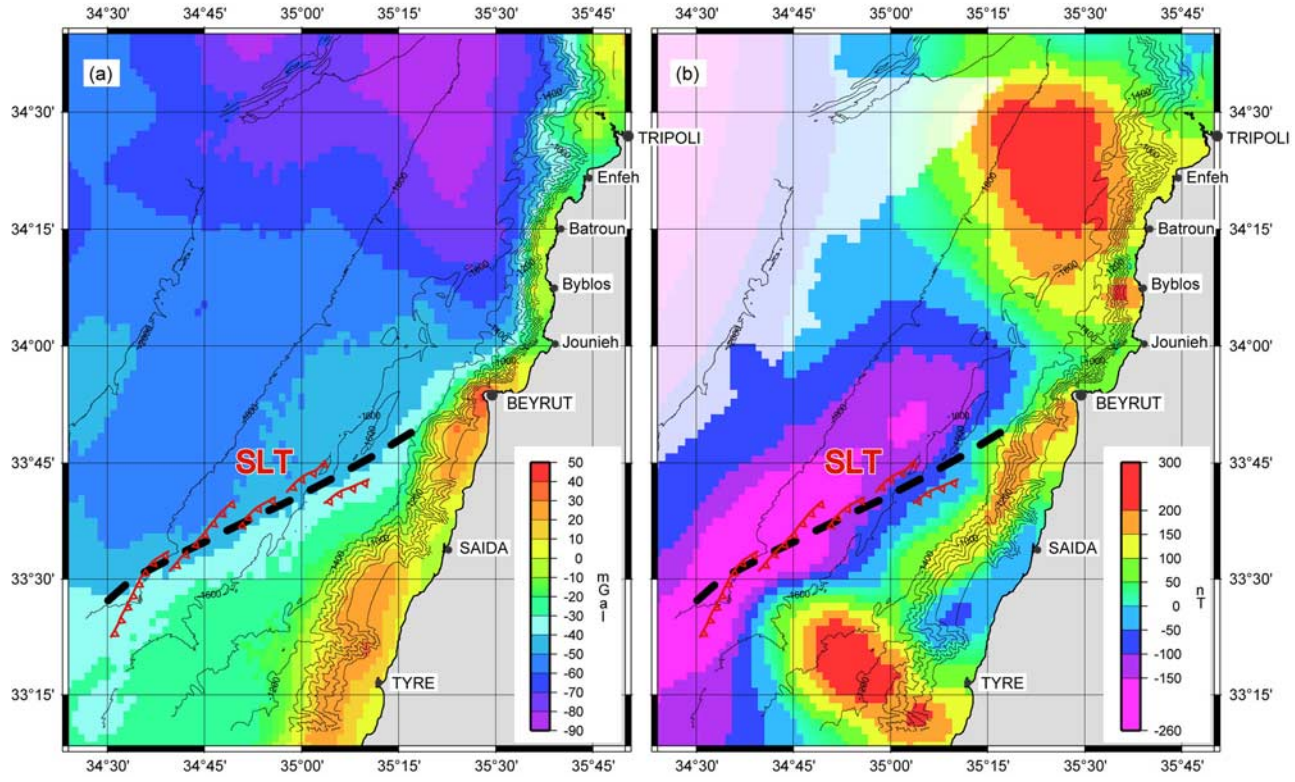

Figure 20. Maps of (a) free-air gravity anomaly in mGal and (b) surface magnetic anomaly in nT. Maps are gridded at 1852-m spacing, with 200-m bathymetric contours superimposed. Free-air gravity anomaly map was compiled from Shalimar shipboard measurements and altimetric data west of 35°E, while no magnetic data were collected in northwestern corner of study area. NE–SW trending boundary extending from Beirut toward the southwest (northern part of the Damietta-Beirut normal fault line in Figure 21a) is marked as a dashed thick black line, with thrust faults of the SLT reactivating this structure in red (other active faults not shown).

oblique thrust ramp, and to the south by a left-stepping branch of the Roum fault, the Saida fault, which both act as lateral ramps of the offshore thrust system. None of these ramps extends farther into the basin, in particular toward Cyprus, which confirms that the Lebanese restraining bend is a self-contained tectonic system [*Tapponnier et al.*, 2001; *Daëron et al.*, 2004; *Elias*, 2006]. Among the few transverse (ENE striking) Mesozoic normal faults [*Dubertret*, 1955] that have been reactivated, with dextral/normal motion, and now accommodate bookshelf-faulting rotation of blocks within Mount Lebanon [*Elias*, 2006], both the Batroun and Nahr El Kelb-Jounieh systems may extend offshore, producing marked discontinuities in the submarine fold-and-thrust belt. Most of the offshore thrusts remain blind, and the clearest examples of reverse faults reaching the surface (and observed in the seismic data) are the extension of the Aabde-Rankine oblique thrust fault in the north and the thrust fault now unambiguously shown to have ruptured during the 551 AD earthquake [*Elias et al.*, 2007], along one of the main slope breaks west and south of Beirut. The interplay between folding and thrusting on the MLT and flow within the Messinian evaporites has created complex shallow deformation patterns that include listric normal faulting and diapiric rise of the salt at places. The evaporite layer also acts as a décollement level, which propagates the shortening seaward through a series of imbricates or duplexes.

7.2. South Lebanon Offshore Thrust System

[36] South of the Mt Lebanon fold-and-thrust belt, the bathymetric slope and the dip of the Messinian erosional surface are more gentle, contrasting with the steep gradients along the central offshore area, which suggests that this southern domain has not been affected by strong nearshore shortening. However, evidence for folding, much of it predating the Quaternary, is observed farther seaward (Figures 5 and 6). One might speculate that folding attributed to the Cretaceous-Eocene Syrian Arc episode on the Israeli margin [*Bertoni and Cartwright*, 2006] might have played a role in shaping offshore Lebanon. But the rare published examples of deep-water "Syrian Arc" folds (such as that sketched by *Frey Martinez et al.* [2005, Figure 9a]) do not affect the Messinian layer. By contrast, the shallow folds imaged in Figures 5 and 6 clearly do and hence cannot be local expressions of a late "Syrian Arc" phase. These folds are mostly aligned along a fault zone that we call the SLT (South Lebanon Thrust). Though segmented, the SLT seems to follow a roughly NE–SW trending boundary (extending from Beirut toward the southwest), which is well expressed in the free-air gravity map (Figure 20a, 40-mGal contour) and also compatible with the magnetic anomaly map (Figure 20b). We interpret this boundary, whose trend is similar to that of large normal faults mapped on land in Mount Lebanon [*Dubertret*, 1955], to represent

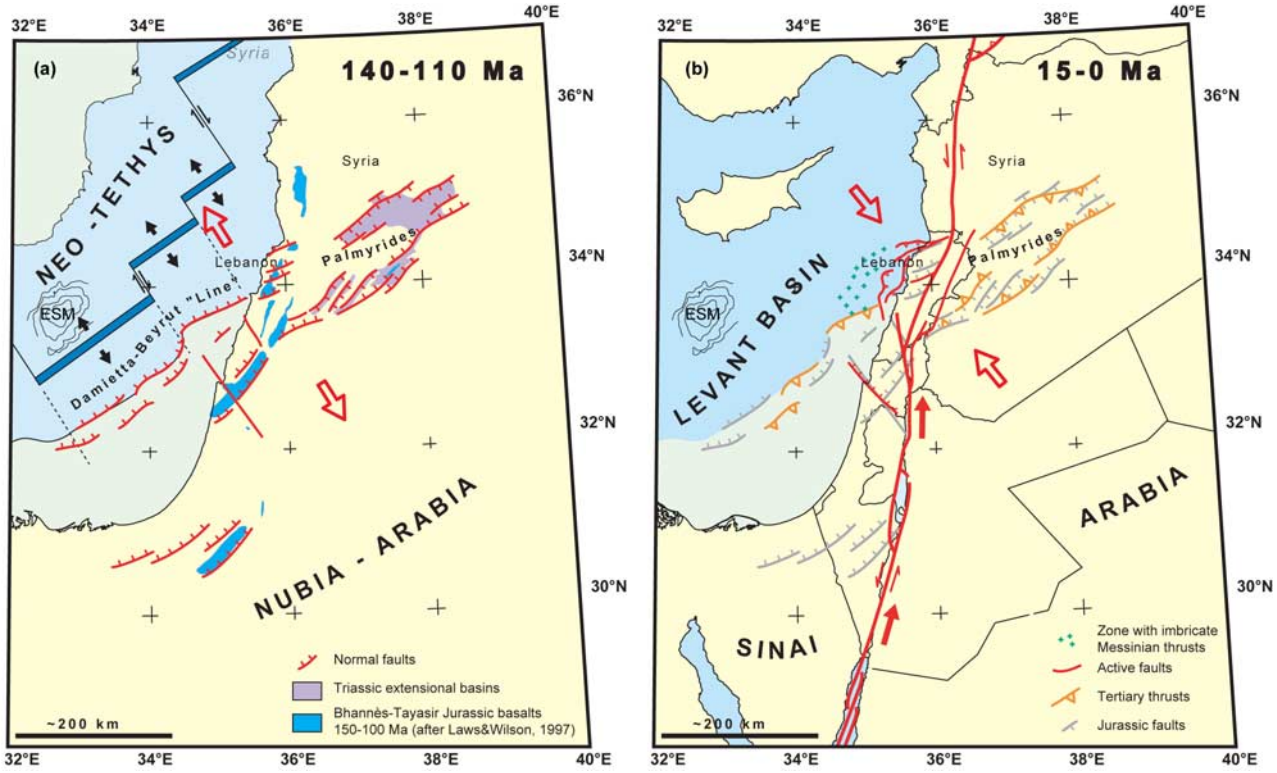

Figure 21. Schematic tectonic evolution of Levant margin from Mesozoic time to present-day configuration, showing inversion along Mount Lebanon segment [after *Tapponnier et al.*, 2004]. (a) At 140–110 Ma, rifting and seafloor spreading in Late Jurassic to Early Cretaceous. (b) At 15–0 Ma, northward propagation of the LFS (red arrows) and formation of Lebanese restraining bend. Northern stretch of LFS is kept very schematic: complexity of fault trace north of Lebanese restraining bend is not represented. Other active structures (Cyprus arc, East Anatolian fault) and connections between them are not shown either. Tertiary thrusts reactivating normal faults along Palmyrides and Damietta-Beyrouth line are marked in orange, late Miocene and active Mount Lebanon Thrust system is marked in red, and zone of imbricate thrusts or duplexes is marked as green crosses. Complete inversion of regional stresses between Cretaceous and Miocene has caused margin inversion and thrust growth of Mount Lebanon megaramp anticline. ESM, Eratosthenes Seamount.

an important regional structure (normal master fault) inherited from the Upper Jurassic to Lower Cretaceous phase of rifting that shaped the Levant passive margin. South of our area of investigation, this NE–SW trending feature seems to follow a line inferred by *Neev et al.* [1985] to continue toward the city of Damietta in the Nile delta. We therefore refer to it as ''Damietta-Beirut line,'' in keeping with its unambiguous termination near Beirut; note that this interpretation differs from the Damietta-Latakia megashear of *Neev et al.* [1985]. In the southern Lebanese offshore area, the SLT forms the western limit of a triangular-shaped area of shallow, irregular seafloor, which coincides with the extensional gravity-spreading domain (Figures 2, 5, and 6). Neither this zone nor extensional salt tectonics exist along the northern offshore area NW of Enfeh and Tripoli. The existence of the SLT being the other main difference between southern and northern Lebanon, this suggests that moderate uplift due to Neogene-recent thrusting might have been responsible for destabilizing the margin, and triggering gravity-driven salt tectonics. Because a continuation of the SLT south of the Shalimar survey area, if any, has not been yet recognized, it is not known whether the salt tectonics observed offshore of Israel has a similar origin. Deep seismic data would be required to characterize the deformation of Miocene layers and test this inference.

7.3. Carmel Fault

[37] The NW striking Carmel fault is a seismically active branch of the LFS [e.g., *Freund et al.*, 1970; *Hofstetter et al.*, 1996] whose onshore trace runs NW from the Dead Sea to the city of Haifa, and likely continues offshore (Figure 7). Near Haifa, the dip-slip component of motion along this fault has been responsible for the uplift of Mount Carmel, a topographic high that coincides with a pronounced magnetic anomaly [*Ben-Avraham and Hall*, 1977; *Ben-Avraham and Ginzburg*, 1990]. The fault has been interpreted as a major boundary separating two distinct crustal domains, Judee-Samaria and Galilee-Lebanon [*Ben-Avraham and Hall*, 1977; *Ben-Avraham*, 1978; *Nur and Ben-Avraham*, 1978]. Shallow seismic reflection profiles acquired in Haifa bay have revealed evidence of active movement along the offshore extension of the fault [*Hübscher et al.*, 2003]. In two recent papers [*Schattner et al.*, 2006; *Ben-Avraham et al.*, 2006], an unpublished copy of the Shalimar bathymetric map was used in conjunction with single-channel seismic data acquired offshore of Lebanon by Israel in 1982, to

propose that the Carmel fault might curve back eastward between the cities of Haifa and Beirut, forming a localized, arcuate fault zone partly embedded within a larger deformation belt linked to salt tectonics. Motion along this arcuate zone has been tentatively inferred to be dominantly left-lateral with local thrusting. Our detailed interpretation of the full bathymetric and seismic reflection data sets of the Shalimar survey suggests instead that the Carmel fault terminates offshore into the NW trending normal fault scarps shown in Figures 7 and 8, forming therefore a horsetail structure around 33°20′N, 34°40′E. We found no sign of a potential transpressive left-lateral connection between the Carmel fault and the SLT zone, whose existence we document convincingly for the first time with the Shalimar data. Thus, former interpretations of the offshore extension of the Carmel fault, such as that proposed by *Ginzburg et al.* [1975], *Garfunkel and Almagor* [1985], and *Ben-Gai and Ben-Avraham* [1995], are more in keeping with the new evidence we provide. Such evidence is also consistent with the dominant NNE–SSW extension direction compatible with the majority of the fault plane solutions determined by *Hofstetter et al.* [1996]. Overall, the Carmel fault zone appears to have played a relatively subordinate role in the recent tectonic evolution of the eastern Levantine basin.

7.4. Passive to Active Margin Inversion

[38] In Figure 21 we propose a schematic two-stage model of the evolution of the Levant margin since the Mesozoic. As recalled in a recent paper by M. Longacre et al. (New crustal structure of the Eastern Mediterranean basin: Detailed integration and modeling of gravity, magnetic, seismic refraction and seismic reflection data, paper presented at EGM 2007 International Workshop, ENI, Capri, Italy, 15–18 April 2007), difficulties persist in constraining seafloor-spreading kinematics in the Levant basin. Figure 21a shows one plausible, if nonunique, solution, in which spreading took place along a roughly NE–SW trending axis segmented by transform faults (drawn perpendicular to the axis for simplicity), and with the basin's eastern margin roughly parallel to the ENE/NE–WSW/SW Tithonian-Neocomian Lebanese normal faults, including the Damietta-Beirut line. Figure 21b illustrates the post-15-Ma evolution of the same area, assuming that the LFS propagated away from the region where its finite offset is largest (the south), that is, northward. While bilateral propagation from both the Gulf of Aqaba and the Taurus-Zagros (as proposed by *Lyakhovsky et al.* [1994]) cannot be ruled out, shortening in the Palmyrides fold belt require that the amount of slip on the northern LFS be smaller than in the south. Figure 21b draws attention to the fact that Lebanon is located roughly where the LFS likely met and interacted with the ENE/NE–SSW/SW striking normal faults that structured the Levant passive margin. We infer the interaction between such inherited structures and the fault to be responsible for the origin of the 160-km-long Lebanese restraining bend. Because it was mechanically easier for the left-lateral Levant fault to follow the weak zone created by faulting along the margin than to slice into the more rigid oceanic lithosphere, it veered eastward at the latitude of southern Lebanon and was deviated along this margin. Consequently, offshore shortening was most pronounced between Saida and Tripoli, while it was much less and occurred earlier south of Saida. Transpression within the bend induced particularly strong reactivation of the ancient passive margin, but such inversion remained local.

[39] Other Mediterranean examples of recent passive margin reactivation over lengths of only 100–200 km are the Algerian margin east of Algiers [*Déverchère et al.*, 2005; *Domzig et al.*, 2006] and the Ligurian margin offshore of the Southern Alps [*Bigot-Cormier et al.*, 2004]. In all three cases, recent shortening has led to similar styles of deformation, due to the presence of the Messinian evaporites: landward dipping blind thrusting, normal faulting at the seafloor formed owing to either hinge extension or gravity spreading, and Plio-Quaternary growth strata.

[40] Our shallow marine seismic profiles alone are not sufficient to constrain the deep geometry of the offshore fault system, but a number of inferences can be drawn. *Daëron* [2005] and *Elias* [2006] suggested that Mount Lebanon should be viewed as a giant ramp anticline, with underthrusting of a sliver of crust along the east dipping MLT. The Shalimar data suggest that the MLT reaches upward closest to the seafloor near the base of the steep bathymetric slope along the central Lebanese offshore area [*Elias et al.*, 2007]. Farther seaward, blind thrust ramps that may merge eastward at depth with the MLT are required to account for the folding of the lower Miocene and Messinian beds, between the slope base and the frontal anticlines, where the evidence for thrusts cutting the base of the Messinian is unmistakable (Figure 9). West of the frontal anticlines, the deformation seems to become dominantly thin-skinned, with a décollement level near the base of the Messinian layer. The profiles do not continue far enough into the basin to sample the full extent of thrust imbrication within the Messinian layer.

7.5. Initiation of Subduction?

[41] In contrast with the reactivation of the Algerian and Ligurian margin, both a direct result of the continuing NS convergence between Africa and Eurasia, the local inversion observed offshore of Lebanon along the eastern passive margin of the Levant basin results from a geometrical irregularity of the Arabia/Sinai transform boundary. This irregularity (a 25° clockwise bend of the Levant fault) is itself a consequence of the encounter between this fault and structures inherited from Neo-Thetysian rifting. At present, with the faulting geometry of the Lebanese restraining bend firmly established, transpression continues at a rate that, though poorly constrained, ranges between 1 and 4 mm/a (3–4.3 mm/a [*Daëron*, 2005], 1–2 mm/a [*Elias*, 2006], 3.0–3.4 mm/a [*Mahmoud et al.*, 2005], and 1.2–2.0 mm/a [*Gomez et al.*, 2007]). Mount Lebanon grows at the expense of southeast directed underthrusting of thickly sedimented, ~110- to 140-Ma-old oceanic or strongly attenuated continental crust [*Dercourt et al.*, 1986; *Ricou*, 1995], with 8-km thickness and 2.8–2.9 density [*Ben-Avraham et al.*, 2002]. Hence, should this process continue, it might result in SE dipping subduction of the Levant oceanic lithosphere. Although no trench is observed along the base of the steep continental slope between Saida and Tripoli, the particularly thick Plio-Quaternary turbidites in the large synclines close to the slope base may be considered to represent the fill of a ~100-km-long flexural foreland basin, deformed by frontal

thrusts whose westward migration has been amplified by the presence of the Messinian evaporites.

[42] The total amount of underthrusting since the middle Miocene (~15 Ma), however, cannot have been more than a few tens of kilometers [*Elias*, 2006] and is thus insufficient to have triggered the kind of buoyancy instability that might enhance subduction and drive its propagation north and south of Lebanon, inverting the entire Levant passive margin into an active one. Besides, the local convergence rate estimated above is less than half that (~1 cm/a) found necessary for subduction to evolve into a self-sustaining system (i.e., controlled by slab pull) by *Toth and Gurnis* [1998].

[43] Nevertheless, the MLT, a 100-km-long megathrust that ruptures during large (M~7.5), infrequent earthquakes [*Elias et al.*, 2007] owing to the underthrusting of oceanic beneath continental lithosphere along one stretch of the western edge of the Arabian plate, fully qualifies as an example of ''induced subduction nucleation,'' even though it is neither a case of ''transference'' nor ''polarity reversal'' [*Stern*, 2004], but rather a novel type of induced nucleation resulting from coastal transpression. Whether localized ''transpressive nucleation'' in the geological past ever resulted in full-fledged subduction, along many hundreds or thousands of kilometers, in the geological past remains to be investigated.

[44] **Acknowledgments.** We thank the captain (G. Ferrand) and crew of R/V *Le Suroît*. The Shalimar (2003) survey was carried out within a French-Lebanese collaboration program, involving and supported by CNRS-Lebanon, IPGP, INSU, CNRS-France, and Ifremer. We are indebted to P. Vidal, J. Ludden, J.-F. Minster, E. Jarmache, M. Hamzé, as well as F. Clavier and J.-N. Baléo, for their invaluable support. We thank Anne-Claire Laurent-Morillon for drawing Figure 21. Reviews by R. Caputo, Z. Ben-Avraham, U. Schattner, and Z. Garfunkel improved earlier versions of the manuscript. This is IPGP contribution 2514.

References

Ambraseys, N. N., and M. Barazangi (1989), The 1759 earthquake in the Bekaa Valley: Implications for earthquake hazard assessment in the Eastern Mediterranean Region, *J. Geophys. Res.*, *94*(B4), 4007–4013, doi:10.1029/JB094iB04p04007.

Ben-Avraham, Z. (1978), The structure and tectonic setting of the Levant continental margin, eastern Mediterranean, *Tectonophysics*, *46*, 313–331, doi:10.1016/0040-1951(78)90210-X.

Ben-Avraham, Z. (1989), Multiple opening and closing of the Eastern Mediterranean and South China basins, *Tectonics*, *8*, 351–362, doi:10.1029/TC008i002p00351.

Ben-Avraham, Z., and A. Ginzburg (1990), Displaced terranes and crustal evolution of the Levant and the eastern Mediterranean, *Tectonics*, *9*, 613–622, doi:10.1029/TC009i004p00613.

Ben-Avraham, Z., and J. K. Hall (1977), Geophysical survey of Mount Carmel structure and its extension into the eastern Mediterranean, *J. Geophys. Res.*, *82*(5), 793–802, doi:10.1029/JB082i005p00793.

Ben-Avraham, Z., A. Ginzburg, J. Makris, and L. Eppelbaum (2002), Crustal structure of the Levant Basin, eastern Mediterranean, *Tectonophysics*, *346*, 23–43, doi:10.1016/S0040-1951(01)00226-8.

Ben-Avraham, Z., U. Schattner, M. Lazar, J. K. Hall, Y. Ben-Gai, D. Neev, and M. Reshef (2006), Segmentation of the Levant continental margin, eastern Mediterranean, *Tectonics*, *25*, TC5002, doi:10.1029/2005TC001824.

Ben-Gai, Y., and Z. Ben-Avraham (1995), Tectonic processes in offshore northern Israel and the evolution of the Carmel structure, *Mar. Pet. Geol.*, *12*, 533–548, doi:10.1016/0264-8172(95)91507-L.

Bertoni, C., and J. A. Cartwright (2006), Controls on the basinwide architecture of late Miocene (Messinian) evaporites on the Levant margin (Eastern Mediterranean), *Sediment. Geol.*, *188–189*, 93–114, doi:10.1016/j.sedgeo.2006.03.019.

Beydoun, Z. R. (1977), Petroleum prospects of Lebanon: Re-evaluation, *AAPG Bull.*, *61*, 43–64.

Bigot-Cormier, F., F. Sage, F. Sosson, J. Déverchère, M. Ferrandini, P. Guennoc, M. Popoff, and J.-F. Stephan (2004), Déformations pliocènes de la marge nord-Ligure (France): les conséquences d'un chevauchement crustal sud-alpin, *Bull. Soc. Geol. Fr.*, *175*, 197–211, doi:10.2113/175.2.197.

Butler, R. W. H., S. Spencer, and H. M. Griffiths (1997), Transcurrent fault activity on the Dead Sea Transform in Lebanon and its implications for plate tectonics and seismic hazard, *J. Geol. Soc.*, *154*, 757–760, doi:10.1144/gsjgs.154.5.0757.

Chaimov, T. A., M. Barazangi, D. Al-Saad, T. Sawaf, and A. Gebran (1990), Crustal shortening in the Palmyride fold belt, Syria, and implications for movement along the Dead Sea fault system, *Tectonics*, *9*, 1369–1386, doi:10.1029/TC009i006p01369.

Chu, D., and R. G. Gordon (1998), Current plate motions across the Red Sea, *Geophys. J. Int.*, *135*, 313–328, doi:10.1046/j.1365-246X.1998.00658.x.

Courtillot, V., R. Armijo, and P. Tapponnier (1987), The Sinai triple junction revisited, *Tectonophysics*, *141*, 181–190, doi:10.1016/0040-1951(87)90184-3.

Daëron, M. (2005), Rôle, cinématique et comportement sismique à long terme de la faille de Yammoûneh, Thèse de doctorat, 178 pp., Inst. de Phys. du Globe de Paris, Paris.

Daëron, M., L. Benedetti, P. Tapponnier, A. Sursock, and R. C. Finkel (2004), Constraints on the post-25-ka slip rate of the Yammouneh fault (Lebanon), using in situ cosmogenic ^{36}Cl dating of offset limestone-clast fans, *Earth Planet. Sci. Lett.*, *227*, 105–119, doi:10.1016/j.epsl.2004.07.014.

Daëron, M., Y. Klinger, P. Tapponnier, A. Elias, E. Jacques, and A. Sursock (2005), Sources of the large A.D. 1202 and 1759 Near East earthquakes, *Geology*, *33*(7), 529–532, doi:10.1130/G21352.1.

Daëron, M., Y. Klinger, P. Tapponnier, A. Elias, E. Jacques, and A. Sursock (2007), 12000-year-long record of 10 to 13 paleoearthquakes on the Yammouneh Fault, Levant Fault System, Lebanon, *Bull. Seismol. Soc. Am.*, *97*(3), 749–771, doi:10.1785/0120060106.

DeMets, C., R. G. Gordon, D. F. Argus, and S. Stein (1994), Effects of recent revisions to the geomagnetic reversal time scale on estimates of current plate motions, *Geophys. Res. Lett.*, *21*, 2191–2194, doi:10.1029/94GL02118.

Dercourt, J., et al. (1986), Geological evolution of the Tethys belt from the Atlantic to the Pamirs since the Lias, *Tectonophysics*, *123*, 241–315, doi:10.1016/0040-1951(86)90199-X.

Déverchère, J., et al. (2005), Active thrust faulting offshore Boumerdes, Algeria, and its relations to the 2003 Mw 6.9 earthquake, *Geophys. Res. Lett.*, *32*, L04311, doi:10.1029/2004GL021646.

Domzig, A., et al. (2006), Searching for Africa-Eurasia Miocene boundary offshore western Algeria (MARADJA'03 cruise), *C. R. Geosci.*, *328*, 80–91.

Dubertret, L. (1955), Carte géologique du Liban, scale 1:200,000, Minist. des Travaux Publics, Beirut.

Elias, A. (2006), Le chevauchement de Tripoli-Saida: Croissance du Mont Liban et risque sismique, Thèse de doctorat, 230 pp., Inst. de Phys. du Globe de Paris, Paris.

Elias, A., et al. (2007), Thrusting offshore Mt Lebanon: Source of the tsunamigenic, 551 AD Beyrut-Tripoli earthquake, *Geology*, *35*(8), 755–758, doi:10.1130/G23631A.1.

Fagin, S. (1998), *Model-Based Depth Imaging*, *Course Note Ser.*, vol. 10, 173 pp., Soc. of Explor. Geophys., Tulsa, Okla.

Fort, X., J.-P. Brun, and F. Chauvel (2004), Salt tectonics on the Angolan margin, synsedimentary deformation processes, *AAPG Bull.*, *88*, 1523–1544, doi:10.1306/06010403012.

Freund, R., I. Zak, and Z. Garfunkel (1968), Age and rate of the sinistral movement along the Dead Sea rift, *Nature*, *220*, 253–255, doi:10.1038/220253a0.

Freund, R., Z. Garfunkel, I. Zak, M. Goldberg, T. Weissbrod, and B. Derin (1970), The shear along the Dead Sea rift, *Philos. Trans. R. Soc. London, Ser. A*, *267*, 107–130, doi:10.1098/rsta.1970.0027.

Frey Martinez, J., J. Cartwright, and B. Hall (2005), 3D seismic interpretation of slump complexes: Examples from the continental margin of Israel, *Basin Res.*, *17*, 83–108, doi:10.1111/j.1365-2117.2005.00255.x.

Garfunkel, Z. (1981), Internal structure of the Dead Sea leaky transform (rift) in relation to plate kinematics, *Tectonophysics*, *80*, 81–108, doi:10.1016/0040-1951(81)90143-8.

Garfunkel, Z. (1984), Large-scale submarine rotational slumps and growth faults in the Eastern Mediterranean, *Mar. Geol.*, *55*, 305–324, doi:10.1016/0025-3227(84)90074-4.

Garfunkel, Z. (1998), Constrains on the origin and history of the Eastern Mediterranean basin, *Tectonophysics*, *298*, 5–35, doi:10.1016/S0040-1951(98)00176-0.

Garfunkel, Z. (2004), Origin of the Eastern Mediterranean basin: A reevaluation, *Tectonophysics*, *391*, 11–34, doi:10.1016/j.tecto.2004.07.006.

Garfunkel, Z., and G. Almagor (1985), Geology and structure of the continental margin off northern Israel and the adjacent parts of the Levantine Basin, *Mar. Geol.*, *62*, 105–131, doi:10.1016/0025-3227(84)90057-4.

Garfunkel, Z., and G. Almagor (1987), Active salt dome development in the Levant Basin, southeastern Mediterranean, in *Dynamical Geology of Salt and Related Structures*, edited by I. Lerche and J. J. O'Brien, pp. 263–300, Academic, Orlando, Fla.

Ginzburg, A., S. S. Cohen, H. Hay-Roe, and A. Rosenzweig (1975), Geology of Mediterranean shelf of Israel, *AAPG Bull.*, *59*, 2142–2160.

Girdler, R. W. (1990), The Dead Sea transform fault system, *Tectonophysics*, *180*, 1–13, doi:10.1016/0040-1951(90)90367-H.

Gomez, F., M. Meghraoui, A. N. Darkal, F. Hijazi, M. Mouty, Y. Suleiman, R. Sbeinati, R. Darawcheh, R. Al-Ghazzi, and M. Barazangi (2003), Holocene faulting and earthquake recurrence along the Serghaya branch of the Dead Sea fault system in Syria and Lebanon, *Geophys. J. Int.*, *153*, 658–674, doi:10.1046/j.1365-246X.2003.01933.x.

Gomez, F., G. Karam, M. Khawlie, S. McClusky, P. Vernant, R. Reilinger, R. Jaafar, C. Tabet, K. Khair, and M. Barazangi (2007), Global Positioning System measurements of strain accumulation and slip transfer trough the restraining bend along the Dead Sea fault system in Lebanon, *Geophys. J. Int.*, *168*, 1021–1028, doi:10.1111/j.1365-246X.2006.03328.x.

Gradmann, S., C. Hübscher, Z. Ben-Avraham, D. Gajevski, and G. Netzeband (2005), Salt tectonics off northern Israel, *Mar. Pet. Geol.*, *22*, 597–611, doi:10.1016/j.marpetgeo.2005.02.001.

Guidoboni, E., F. Bernardini, A. Comastri, and E. Boschi (2004), The large earthquake on 29 June 1170 (Syria, Lebanon, and central southern Turkey), *J. Geophys. Res.*, *109*, B07304, doi:10.1029/2003JB002523.

Hall, J., T. J. Calon, A. E. Aksu, and S. R. Meade (2005), Structural evolution of the Latakia Ridge and Cyprus Basin at the front of the Cyprus Arc, eastern Mediterranean Sea, *Mar. Geol.*, *221*, 261–291, doi:10.1016/j.margeo.2005.03.007.

Hofstetter, A., T. Van Eck, and A. Shapira (1996), Seismic activity along fault branches of the Dead Sea-Jordan Transform System: The Carmel-Tirtza fault system, *Tectonophysics*, *267*, 317–330, doi:10.1016/S0040-1951(96)00108-4.

Hübscher, C., Z. Ben-Avraham, A. Dehghani, and K. Gohl (2003), New geophysical data from the southern Levantine continental margin and outer Nile cone: The GEMME project, *Geophys. Res. Abstr.*, *5*, 03592.

Joffe, S., and Z. Garfunkel (1987), Plate kinematics of the circum Red Sea: A re-evaluation, *Tectonophysics*, *141*, 5–22, doi:10.1016/0040-1951(87)90171-5.

Khair, K. (2001), Geomorphology and seismicity of the Roum fault as one of the active branches of the Dead Sea fault system in Lebanon, *J. Geophys. Res.*, *106*(B3), 4233–4245, doi:10.1029/2000JB900287.

Laws, E. D., and M. Wilson (1997), Tectonics and magmatism associated with Mesozoic passive continental margin development in the Middle East, *J. Geol. Soc.*, *154*(3), 459–464, doi:10.1144/gsjgs.154.3.0459.

Lyakhovsky, V., Z. Ben-Avraham, and M. Achmon (1994), The origin of the Dead Sea rift, *Tectonophysics*, *240*, 29–43, doi:10.1016/0040-1951(94)90262-3.

Mahmoud, S., R. Reilinger, S. McClusky, P. Vernant, and A. Tealeb (2005), GPS evidence for northward motion of the Sinai Block: Implications for E. Mediterranean tectonics, *Earth Planet. Sci. Lett.*, *238*, 217–224, doi:10.1016/j.epsl.2005.06.063.

Makris, J., Z. Ben-Avraham, A. Behle, A. Ginzburg, P. Giese, L. Steinmetz, R. B. Whitmarsh, and S. Eleftheriou (1983), Seismic refraction profiles between Cyprus and Israel and their interpretation, *Geophys. J. R. Astron. Soc.*, *75*, 575–591.

Manighetti, I., P. Tapponnier, P.-Y. Gillot, E. Jacques, V. Courtillot, R. Armijo, J.-C. Ruegg, and G. King (1998), Propagation of rifting along the Arabia-Somalia plate boundary: Into Afar, *J. Geophys. Res.*, *103*(B3), 4947–4974, doi:10.1029/97JB02758.

Mart, Y., and W. Ryan (2007), The Levant slumps and the Phoenician structures: Collapse features along the continental margin of the southeastern Mediterranean Sea, *Mar. Geophys. Res.*, *28*, 297–307, doi:10.1007/s11001-007-9032-7.

Mauduit, T., and J.-P. Brun (1998), Growth fault/rollover systems: Birth, growth and decay, *J. Geophys. Res.*, *103*, 18,119–18,136, doi:10.1029/97JB02484.

McClusky, S., R. Reilinger, S. Mahmoud, D. Ben Sari, and A. Tealeb (2003), GPS constraints on Africa (Nubia) and Arabia plate motions, *Geophys. J. Int.*, *155*, 126–138, doi:10.1046/j.1365-246X.2003.02023.x.

McKenzie, D. P. (1972), Active tectonics of the Mediterranean region, *Geophys. J. R. Astron. Soc.*, *30*, 109–185.

Morhange, C., P. A. Pirazzoli, N. Marriner, L. F. Montaggioni, and T. Nammour (2006), Late Holocene relative sea-level changes in Lebanon, eastern Mediterranean, *Mar. Geol.*, *230*, 99–114, doi:10.1016/j.margeo.2006.04.003.

Neev, D., L. L. Greenfield, and J. K. Hall (1985), Slice tectonics in the Eastern Mediterranean Basin, in *Geological Evolution of the Mediterranean Basin*, edited by D. J. Syanley and F. D. Wezel, pp. 249–269, Springer, New York.

Nemer, T., and M. Meghraoui (2006), Evidence of coseismic ruptures along the Roum fault (Lebanon): A possible source for the AD 1837 earthquake, *J. Struct. Geol.*, *28*, 1483–1495, doi:10.1016/j.jsg.2006.03.038.

Netzeband, G., K. Gohl, C. P. Hübscher, Z. Ben-Avraham, G. A. Dehghani, D. Gajewski, and P. Liersch (2006a), The Levantine Basin: Crustal structure and origin, *Tectonophysics*, *418*, 167–188, doi:10.1016/j.tecto.2006.01.001.

Netzeband, G., C. P. Hübscher, and D. Gajevski (2006b), The structural evolution of the Messinian evaporites in the Levantine Basin, *Mar. Geol.*, *230*, 249–273, doi:10.1016/j.margeo.2006.05.004.

Nur, A., and Z. Ben-Avraham (1978), The eastern Mediterranean and the Levant: Tectonics of continental collision, *Tectonophysics*, *46*, 297–312, doi:10.1016/0040-1951(78)90209-3.

Ricou, L. E. (1995), The plate tectonics history of the past Tethys Ocean, in *The Oceans Basins and Margins*, vol. 8, *The Tethys Ocean*, edited by A. E. M. Nairn et al., pp. 3–70, Plenum, New York.

Robertson, A. H. F. and the Leg ODP 160 Shipboard Scientific Party (1996), Tectonic introduction, *Proc. Ocean Drill. Program Initial Rep.*, *160*, 5–18.

Ryan, W. B. F., D. J. Stanley, J. B. Hersey, D. A. Fahlquist, and T. D. Allan (1970), The tectonics and geology of the Mediterranean Sea, *The Sea*, vol. 4, edited by A. E. Maxwell, pp. 387–492, John Wiley, New York.

Sanlaville, P. (1977), Etude géomorphologique de la région littorale du Liban, Ph.D. thesis, 859 pp., Lebanese Univ., Beirut.

Schattner, U., Z. Ben-Avraham, M. Lazar, and C. Hübscher (2006), Tectonic isolation of the Levant basin offshore Galilee-Lebanon: Effects of the Dead Sea fault plate boundary on the Levant continental margin, eastern Mediterranean, *J. Struct. Geol.*, *28*, 2049–2066, doi:10.1016/j.jsg.2006.06.003.

Stern, R. J. (2004), Subduction initiation: Spontaneous and induced, *Earth Planet. Sci. Lett.*, *226*, 275–292.

Tapponnier, P., M. Daëron, G. King, E. Jacques, A. Sursock, and A. Elias (2001), Active faulting and seismic hazard in Lebanon, *J. Conf. Abstr.*, *6*, 296.

Tapponnier, P., A. Elias, A. Sursock, R. Jomaa, A. Briais, H. Carton, S. Singh, M. Daëron, G. King, and E. Jacques (2004), Passive-active margin inversion on the Levant plate boundary: subduction birth and growth of Mt Lebanon, *Eos. Trans. AGU*, *85*(47), Fall Meet.Suppl., Abstract T52B-05.

Toth, J., and M. Gurnis (1998), Dynamics of subduction initiation at preexisting fault zones, *J. Geophys. Res.*, *103*(B8), 18,053–18,067, doi:10.1029/98JB01076.

Vendeville, B., and P. R. Cobbold (1987), Glissements gravitaires sysnsédimentaires et failles normales listriques: Modèles expérimentaux, *C. R. Acad. Sci.*, *305*, 1313–1319.

Vidal, N., J. Alvares-Marron, and D. Klaeschen (2000), Internal configuration of the Levantine Basin from seismic reflection data, *Earth Planet. Sci. Lett.*, *180*, 77–89, doi:10.1016/S0012-821X(00)00146-1.

Walley, C. D. (1998), Some outstanding issues in the geology of Lebanon and their importance in the tectonic evolution of the Levantine region, *Tectonophysics*, *298*, 37–62, doi:10.1016/S0040-1951(98)00177-2.

L. Barrier, E. Jacques, G. C. P. King, and P. Tapponnier, Equipe de Tectonique, Institut de Physique du Globe de Paris, 4 Place Jussieu, F-75252 Paris CEDEX 05, France.

A. Briais, Laboratoire de Dynamique Terrestre et Planétaire, Observatoire Midi-Pyrénées, 14 Avenue Edouard Belin, F-31400 Toulouse, France.

H. Carton, Lamont-Doherty Earth Observatory, Earth Institute at Columbia University, 61 Route 9W, Palisades, NY 10964, USA.

M. Daëron, Laboratoire des Sciences du Climat et de l'Environnement, Avenue de la Terrasse, F-91198 Gif-sur-Yvette, France.

A. Elias, Geology Department, American University of Beirut, P.O. Box 11-0236, Riad El-Solh, 1107 2020 Beirut, Lebanon.

R. Jomaa and A. Sursock, National Center for Geophysical Research, P.O. Box 11-8281, Riad El-Solh, 1107 2260 Beirut, Lebanon.

S. C. Singh, Equipe de Géosciences Marines, Institut de Physique du Globe de Paris, 4 Place Jussieu, F-75252 Paris CEDEX 05, France.